NASA-CR-168269

NASA Contractor Report 168269

USERS' MANUAL FOR COMPUTER PROGRAM FOR THREE-DIMENSIONAL ANALYSIS OF COUPLED-CAVITY TRAVELING WAVE TUBES

by Thomas A. O'Malley

Analex Corporation
Cleveland, Ohio 44135

January 1984

Prepared for

NATIONAL AERONAUTICS AND SPACE ADMINISTRATION
Lewis Research Center
Under Contract NAS 3-23293

ENTER:
5 1 1 RN/NASA-CR-168269
DISPLAY 05/2/1
84N23841*# ISSUE 14 PAGE 2141 CATEGORY 33 RPT#: NASA-CR-168269
E-1930 NAS 1.26:168269 CNT#: NAS3-23293 84/01/00 66 PAGES
UNCLASSIFIED DOCUMENT
UTTL: Users' manual for computer program for three-dimensional analysis of coupler-cavity traveling wave tubes TLSP: Final Report
AUTH: A/OMALLEY, T. A.
CORP: Analex Corp., Cleveland, Ohio. AVAIL.NTIS SAP: HC A04/MF A01
MAJS: /*COMPUTER AIDED DESIGN/*COMPUTER PROGRAMS/*COMPUTERIZED SIMULATION/* SPACECRAFT COMMUNICATION/*TRAVELING WAVE TUBES/*USER MANUALS (COMPUTER PROGRAMS)
MINS: / COUPLERS/ CURRENT DENSITY/ DATA CONVERSION ROUTINES/ ELECTRIC FIELDS/ FOURIER ANALYSIS/ IBM 370 COMPUTER/ SPACE CHARGE
ABA: M.A.C.
ABS: The use of the coupled cavity traveling wave tube for space communications has led to an increased interest in improving the efficiency of the basic interaction process in these devices through velocity resynchronization and other methods. A flexible, three dimensional, axially symmetric, large signal computer program was developed for use on the IBM 370 time sharing system. A users' manual for this program is included.

ENTER:

CONTENTS

	Page
SUMMARY	1
INTRODUCTION	1
MODEL OF COUPLED-CAVITY TRAVELING WAVE TUBE	2
PROGRAM STRUCTURE	4
Dynamics of Beam Rings	4
Equations of motion	4
Initial conditions	7
Space charge forces	8
Radiofrequency electric field forces	15
Voltage-jump electric field forces	17
Magnetic field forces	18
Rings with small radius	21
Beam-Wave Coupling Analysis	24
Summary of Program Steps	29
DESCRIPTION OF INPUT DATA	29
DESCRIPTION OF OUTPUT DATA	33
DESCRIPTION OF GLOBAL VARIABLES	35
DESCRIPTION OF SUBROUTINES	41
COMMON Blocks	41
Main Program	41
Subroutine ACC	42
Subroutine APPLE	42
Subroutine BTOS	42
Subroutine BTWNC	42
Subroutine BTWNS	43
Subroutine CAVP	43
Subroutine CKPDZ	43
Subroutine CROOT	43
Subroutine DVSUM	43
Subroutine ENBAL	43
Subroutine FACC1	44
Subroutine FACC3	44
Subroutine FIELD	44
Subroutine FSAPP	44
Subroutine INDAT	44
Subroutine INIT	45
Subroutine INTRC	45
Subroutine MAGCF	46
Subroutine NBEAM	46
Subroutine OUTPT	46
Subroutine PLOTS	46
Subroutine SACC1	47
Subroutine SACC3	47

Subroutine SCAT1 47
Subroutine SCAT3 47
Subroutine SCFT1 48
Subroutine SCFT3 48
Subroutine SMSIG 48
Subroutine STDAT 48
Subroutine STOB 49
Subroutine TABL1 49
Subroutine TBL3E 49
Subroutine TBL3M 49
Subroutine TRN13 50
Subroutine XINT 50

CONCLUDING REMARKS 50

APPENDIXES
A - SYMBOLS 51
B - DERIVATION OF FOURIER COMPONENT OF BEAM CURRENT DENSITY 53

REFERENCES 56

USERS' MANUAL FOR COMPUTER PROGRAM FOR THREE-DIMENSIONAL ANALYSIS OF COUPLED-CAVITY TRAVELING WAVE TUBES

Thomas A. O'Malley

Analex Corporation
Cleveland, Ohio 44135

SUMMARY

The use of the coupled-cavity traveling wave tube (TWT) for space communications has led to an increased interest in the efficiency of these devices. Efficiency improvements have generally been along two lines: (1) the development of efficient multistage depressed collectors to recover a high percentage of the kinetic power in the spent beam; and (2) improvements in the efficiency of the basic interaction process through velocity resynchronization and other methods. To pursue the second line, we have recently developed a flexible, three-dimensional, axially-symmetric, large-signal computer program written in FORTRAN IV for use on the IBM 370 time-sharing system. The present report is a users' manual for this program.

The basic programming approach consists of dividing the beam into rings and calculating the trajectories of these rings as they pass through a sequence of cavities each of which may have different geometrical and electrical properties. Extreme flexibility is provided in the variety of tube features that can be modeled since each cavity has individually entered input parameters. The program can handle lumped or distributed severs, input and output couplers, cavity match details provided for cavities near the end of a stack, voltage-jump velocity resynchronization with an arbitrary number of discrete steps (up to one per cavity), and velocity taper designs of almost arbitrary complexity. Backward waves can be handled by an interative procedure.

INTRODUCTION

The use of the coupled-cavity traveling wave tube (TWT) for space communications has led to an increased interest in the efficiency of these devices. Efficiency improvements have generally been along two lines: (1) the development of efficient multistage depressed collectors to recover a high percentage of the kinetic power in the spent beam; and (2) improvements in the efficiency of the basic interaction process through velocity resynchronization and other methods. The NASA Lewis Research Center has been interested in the first approach to efficiency enhancement for sometime (refs. 1 to 3). In the second approach, we have developed a flexible, one-dimensional, large-signal computer program (refs. 4 to 6). This computer program, because of the limitations of one-dimensional motion, is not highly accurate in its calculation of electron trajectories or beam-wave interaction. Also, one-dimensional motion does not allow calculation of beam interception or vector velocities of electrons. Beam interception data is required in order to determine the properties required of an effective magnetic focusing system. Vector velocity data is particularly important in the design of efficient collectors. The vector

velocities at the output of the tube are required as input data to a computer program which analyzes collectors.

Because of the need to overcome the aforementioned limitations inherent in a one-dimensional program, we have recently developed a three-dimensional program written in FORTRAN IV. This program retains all of the features in the one-dimensional program and is essentially a generalization of that program to a three-dimensional, axially-symmetric simulation.

The basic programming approach is to follow a ring-model beam through a sequence of cavities each of which may have different geometrical and electrical properties. Extreme flexibility is provided in the variety of tube features that can be modeled since each cavity has individually entered input parameters. The program can handle lumped or distributed severs, input and output couplers, cavity match details provided for cavities near the end of a stack, voltage-jump velocity resynchronization with an arbitrary number of discrete steps (up to one per cavity) and velocity taper designs of almost arbitrary complexity. Backward waves can be handled by an iterative procedure similar to that described by Kino, et al. (ref. 7).

In this report, we first discuss the computer model of the coupled-cavity TWT. A detailed discussion of the program structure follows. The input data, output data, program variables, and program subroutines are then described.

MODEL OF COUPLED-CAVITY TWT

The model of a coupled-cavity TWT is illustrated in figure 1. The beam is divided into a series of disks, and each disk is subdivided into an arbitrary number of rings. A complete description of the beam trajectory is obtained by following the rings contained in a single beam wavelength (ref. 8). The rings may penetrate each other in both the radial and axial directions. The rings expand or contract radially according to the radial forces acting on them. The rings do <u>not</u> contract or expand in the axial direction; the axial thickness of a ring is assumed to be constant. Also the rings do not become warped; that is, the trace of a ring in the r-z plane is always a rectangle.

The axial and radial thickness of a ring comes into play only in the modeling of beam interception and in the calculation of space charge forces. For all other forces, it is assumed that the charge and mass of a ring are concentrated at the ring's centroid radius and that the ring has zero axial thickness.

Each ring, as it enters the tube, has a charge equal to $1/R$ of the charge of the disk, where R is the number of rings per disk. Also the initial cross-sectional area is the same for all rings. For the case of $R = 3$, the ring dimensions at the tube entrance are given in figure 2. The axial thickness ℓ_d of all rings is λ_e/N_d, where λ_e is the beam wavelength and N_d is the number of disks in a beam wavelength.

For an arbitrary value of R, we have

$$r_j = \sqrt{\frac{2j - 1}{2R}}\, b, \qquad j = 1, \ldots, R \tag{1}$$

$$r_{in,j} = \sqrt{\frac{2j-2}{2j-1}}\, r_j, \qquad j = 1, \ldots, R \tag{2}$$

$$r_{out,j} = \sqrt{\frac{2j}{2j-1}}\, r_j, \qquad j = 1, \ldots, R \tag{3}$$

In modeling beam interception, we must make assumptions on the values of the inner and outer radii, given the value of the centroid radius. The assumption is that the ratio of the inner radius to centroid radius and the ratio of the outer radius to centroid radius remain constant. These ratios are determined from equations (2) and (3). At the end of an integration step, if the outer radius of a ring exceeds the tunnel radius a, then the outer radius is redefined to be a, and the portion of the ring located beyond $r = a$ is assumed to be intercepted. The remaining partial ring, since its outer radius has been redefined, has a redefined value of centroid radius given by

$$r_j = \sqrt{\frac{r_{in,j}^2 + r_{out,j}^2}{2}}, \qquad j = 1, \ldots, R \tag{4}$$

The program has an option allowing a one-dimensional beam to be used in the first N cavities, where N is an input parameter, and a switch is then made to a three-dimensional simulation. The results for the first N cavities would be nearly identical to those of the one-dimensional program described in reference 4 because the same model is used in both programs. This report will discuss only the three-dimensional model since the one-dimensional model is thoroughly documented in references 4 and 5. A basic understanding of references 4 and 5 is presupposed in this report. The tube body is treated as a conducting tunnel of radius a divided axially into a series of discrete cells, where the length of the k^{th} cell is denoted by L_k. In the center of each cell is a gap of length $2\ell_k$. Impressed across the k^{th} gap is a complex voltage $V_k e^{i\omega t}$.

In the absence of a beam, there will be a simple known relation among the various V_k. For a forward-propagating wave in the pass band of a uniform structure,

$$V_{k+1} = e^{-(\alpha + i\beta_1)L_k} V_k \tag{5}$$

where α and β_1 are known from cold-test measurements. The power flowing along the structure will be given by

$$P_k = \frac{|V_k|^2}{2Z_k} \tag{6}$$

where Z_k also is known from cold-test measurements.

The voltage wave in the presence of the beam is calculated by adding a complex induced voltage to the propagating wave, that is,

$$V_{k+1} = e^{-(\alpha+i\beta_1)L_k} V_k + \Delta V_{k+1} \tag{7}$$

where ΔV_{k+1} is an induced voltage to be defined later.

The body of a coupled-cavity TWT is supposedly a periodic structure. If this were the case, all cavities would have the same L, ℓ, αL, $\beta_1 L$, and Z. However, a real tube has input and output couplers, severs, and perhaps velocity tapers and cavity match details, all of which require individual non-periodic treatment in the model. Thus, the properties of individual cavities are separately specified input parameters in the program, and a great variety of tube design variations such as complicated velocity tapers or voltage-jump configurations can be easily modeled. Equation (7) is easily modified to handle such a quasi-periodic structure,

$$V_{k+1} = \tau_k \sqrt{\frac{Z_{k+1}}{Z_k}} V_k + \Delta V_{k+1}$$

where

$$\tau_k = e^{-(\alpha L)_k} e^{-i(\beta_1 L)_k}$$

The factor $\sqrt{Z_{k+1}/Z_k}$ ensures that power flow is conserved.

PROGRAM STRUCTURE

The program consists of two major elements: the dynamics of the beam rings and the beam-wave coupling analysis. These two elements are described in detail in the following sections.

Dynamics of Beam Rings

Equations of motion. - As discussed in reference 4, page 4, it is more convenient to let the independent variable be the axial position z rather than the time t, and we calculate the functions $r(z)$ and $t(z)$. Here $r(z)$ is the centroid radius of the ring in question when it reaches the axial position z, and $t(z)$ is the time of arrival of the ring at the axial position z. The transformation from equations of motion with t as independent variable to equations of motion with z as independent variable is given by

$$\frac{d^2t}{dz^2} = \frac{-\frac{d^2z}{dt^2}}{\left(\frac{dz}{dt}\right)^3} \tag{8}$$

$$\frac{d^2r}{dz^2} = \frac{\frac{d^2r}{dt^2} - \frac{d^2z}{dt^2}\frac{dr}{dz}}{\left(\frac{dz}{dt}\right)^2} \tag{9}$$

Instead of using t, z, and r, we use the normalized variables Θ, ξ, and ρ defined by

$$\Theta = \omega t \tag{10}$$

$$\xi = \frac{z}{a} \tag{11}$$

$$\rho = \frac{r}{a} \tag{12}$$

In terms of the normalized variables, the transformation equations are

$$\frac{d^2\Theta}{d\xi^2} = \frac{-\frac{d^2\xi}{d\Theta^2}}{\left(\frac{d\xi}{d\Theta}\right)^3} \tag{13}$$

$$\frac{d^2\rho}{d\xi^2} = \frac{\frac{d^2\rho}{d\Theta^2} - \frac{d^2\xi}{d\Theta^2}\frac{d\rho}{d\xi}}{\left(\frac{d\xi}{d\Theta}\right)^2} \tag{14}$$

Although the normalized variables are used in the program, the unnormalized variables will be used in any explanation for which greater clarity can be achieved. At each integration step, the usual equations of motion with t as independent variable are used to calculate d^2z/dt^2 and d^2r/dt^2. Knowing these quantities, we then calculate d^2t/dz^2 and d^2r/dz^2 from equations (8) and (9).

The equations of motion with t as independent variable may be in either relativistic or nonrelativistic form. The equations for d^2z/dt^2 and d^2r/dt^2 for the ring in question are

$$\frac{d^2z}{dt^2} = \beta\left\{\frac{q}{m}\left(E_{rf,z} + E_{sc,z} - r\dot{\phi}B_r\right) + U_z\right\} \tag{15}$$

$$\frac{d^2r}{dt^2} = \beta\left\{\frac{q}{m}\left(E_{rf,r} + E_{sc,r} + r\dot{\phi}B_z\right) + \frac{1}{\beta}r\dot{\phi}^2 + U_r\right\} \tag{16}$$

where $\dot{\phi}$ is the angular velocity of the ring and β is defined as

$$\beta = 1 \text{ (nonrelativistic case)}$$

$$\beta = \sqrt{1 - \frac{v^2}{c^2}} \text{ (relativistic case)} \tag{17}$$

In the above equations, B_z and B_r are the axial and radial components of the magnetic induction at the location of the ring, $E_{rf,z}$ and $E_{rf,r}$ are the components of the rf electric field, and $E_{sc,z}$ and $E_{sc,r}$ are the components of the space-charge field. For the nonrelativistic case, U_z and U_r are zero. For the relativistic case, U_z and U_r are complex expressions involving a factor W defined as

$$W = \frac{-q}{m\omega^2 c^2 a}\left\{\frac{dr}{dt}\left(E_{rf,r} + E_{sc,r}\right) + \frac{dz}{dt}\left(E_{rf,z} + E_{sc,z}\right)\right\} \tag{18}$$

where ω is the angular frequency. U_z and U_r are then given by

$$U_z = W\frac{dz}{dt} + \frac{q}{m}\frac{dr}{dt}\frac{B_\phi}{\omega} \tag{19}$$

$$U_r = W\frac{dr}{dt} - \frac{q}{m}\frac{dz}{dt}\frac{B_\phi}{\omega} \tag{20}$$

where B_ϕ is the azimuthal magnetic induction given by

$$B_\phi = \frac{-\mu_o I_{o,ave}\, r}{2\pi r_{max}^2} \tag{21}$$

In the above expression, μ_o is the permeability of free space, r_{max} is the outer radius of the outermost ring, and $I_{o,ave}$ is the average beam current.

The angular velocity $\dot{\phi}$ of the ring is given by

$$\dot{\phi} = \dot{\phi}_o - \frac{q}{m}\left[\frac{\psi(r,z) - \psi(r_o,z_o)}{2\pi r^2}\right]\beta \tag{22}$$

where $\psi(r,z)$ is the magnetic flux at the ring location (r,z), and the subscript o denotes conditions at the tube entrance.

The coordinate system used in the program has its origin at the beginning of the first cavity. The k^{th} cavity is divided into N_z equal parts of length Δz_k, given by

$$\Delta z_k = \frac{L_k}{N_z}$$

The n^{th} node in the first cavity, denozed by z_{n1}, is defined by

$$z_{n1} = \left(n - \frac{1}{2}\right)\Delta z_1 \qquad n = 1, \ldots, N_z \tag{23}$$

The n^{th} node in the k^{th} cavity, denoted by z_{nk}, is given by

$$z_{nk} = \sum_{m=1}^{k-1} L_m + \left(n - \frac{1}{2}\right)\Delta z_k \qquad \begin{cases} n = 1, \ldots, N_z \\ k = 2, \ldots, N_c \end{cases} \tag{24}$$

where N_c is the number of cavities. A point that lies midway between two nodes $z_{n,k}$ and $z_{n+1,k}$ is denoted by $z_{n+1/2,k}$. Such a point is called the n^{th} antinode in cavity k (fig. 3). The numerical integration of equations (8) and (9) for the i^{th} ring is such that $t_i(z)$ and $r_i(z)$ and the first derivatives of these functions are evaluated at antinodes, and the second derivatives are evaluated at nodes. The numerical integration scheme is the same as that described in reference 4, equations (8) to (11), for calculating $t_i(z)$. The identical scheme is used for calculating $r_i(z)$.

The numerical integration method used here is not as accurate, for a fixed step size, as the widely used Runge-Kutta methods or predictor-corrector methods. The advantage of the method used here is that it requires evaluating accelerations only once per integration step, whereas the other methods requires evaluating accelerations at least twice per integration step. To be competitive with the method used here, another method requiring evaluation of accelerations twice per step would have to achieve comparable accuracy with double the step size. Such a comparison between the method used here and a Runge-Kutta method requiring evaluation of accelerations twice per step has been made. The method used here achieved the greater accuracy.

Initial conditions. - At times it is convenient to use a single subscript to denote the ring number; for example, $t_i(z)$ would denote the time of arrival of the i^{th} ring at the axial position z, where i runs from 1 to RN_d. At other times it is convenient to use a double subscript to denote the ring number; for example, $t_{ij}(z)$ would denote the time of arrival of the ring which originally was the j^{th} ring making up the i^{th} disk, where j runs from 1 to R and i runs from 1 to N_d.

The initial total velocity of all rings is

$$u_{ji,o} = u_o = c\sqrt{1 - \frac{1}{\left(1 + \frac{\left|\frac{q_{ji}}{m_{ji}}\right| V_o}{c^2}\right)^2}} \qquad \begin{cases} j = 1, \ldots, R \\ i = 1, \ldots, N_d \end{cases} \tag{25}$$

where c is the velocity of light, $|q_{ji}/m_{ji}|$ is the charge-to-mass ratio, and V_o is the beam voltage. The initial angular velocity of all the rings is

$$\dot{\phi}_{ji,o} = \dot{\phi}_o = \frac{\frac{-q_{ji}}{m_{ji}}\psi_c}{2\pi r_{Ri,o}^2} \qquad \begin{cases} j = 1, \ldots, R \\ i = 1, \ldots, N_d \end{cases} \tag{26}$$

where ψ_c is the cathode flux at an outermost ring and $r_{Ri,o}$ is the initial radius of an outermost ring. The initial axial velocity is

$$\dot{z}_{ji,o} = \sqrt{u_o^2 - (r_{ji,o}\,\dot{\phi}_o)^2} \qquad \begin{cases} j = 1, \ldots, R \\ i = 1, \ldots, N_d \end{cases} \tag{27}$$

where $r_{ji,o}$ is the initial radius of the $(j,i)^{th}$ ring. From equation (27), $\dot{z}_{ji}$ is not the same for all rings. It is the largest for the innermost rings and the smallest for the outermost rings. It follows that the beam wavelength, defined as $\dot{z}_{ji,o}$ divided by frequency, is not the same for all rings. This is an inconvenience we wish to avoid, so we assign to $\dot{z}_{ji,o}$ the value it would have if R were equal to 1.

$$\dot{z}_{ji,o} = \dot{z}_o = \sqrt{u_o^2 - \left(\frac{\sqrt{2}}{2}\, b\, \dot{\phi}_o\right)^2} \tag{28}$$

where b is the initial beam radius.

Since $t_{ji}(z)$ and $r_{ji}(z)$ are the trajectory functions to be calculated, we must specify the initial values of these functions and their first derivatives. These are given by

$$t_{ji} = \frac{(i-1)\ell_d}{\dot{z}_o} \tag{29}$$

$$r_{ji} = \sqrt{\frac{2j-1}{2R}}\, b \tag{30}$$

$$\frac{dt_{ji}}{dz} = \frac{1}{\dot{z}_o} \tag{31}$$

$$\frac{dr_{ji}}{dz} = 0 \tag{32}$$

$$j = 1, \ldots, R; \quad i = 1, \ldots, N_d$$

For some applications dr_{ji}/dz is nonzero. For such cases, dr_{ji}/dz is specified in the input data.

Space charge forces. - The starting point in developing the space-charge model is an expression for the potential field due to a point charge q in a cylindrical tunnel. From reference 5, equation (10), the potential at (r_2, ϕ_2, z) is

$$V(r_2,\phi_2,z) = \frac{q}{2\pi\epsilon_0 a^2} \sum_{\substack{m=1 \\ s=0}}^{\infty} (2 - \delta_{so}) e^{-\mu_{ms}|z|} \cos s(\phi_2 - \phi_1) \frac{J_s(\mu_{ms} r_2) J_s(\mu_{ms} r_1)}{\mu_{ms}[J_{s+1}(\mu_{ms} a)]^2} \tag{33}$$

where a is the tunnel radius, ϵ_0 is the permittivity of free space, and

$$J_s(\mu_{ms} a) = 0, \qquad \delta_{so} = \begin{cases} 1 \text{ for } s = 0 \\ 0 \text{ for } s \neq 0 \end{cases} \tag{34}$$

and the charge is located at $(r_1,\phi_1,0)$. We can obtain the electric field set up by the point charge from the equation $E = -\nabla V$. By a simple integration, we can then find the electric field due to a charged ring of charge q_1 and radius r_1. The field at (r_2,z) is

$$E_z(r_2,z) = \frac{\mathrm{sgn}(z) q_1}{2\pi\epsilon_0 a^2} \sum_{m=1}^{\infty} \frac{J_0(\mu_m r_1) J_0(\mu_m r_2)}{[J_1(\mu_m a)]^2} e^{-\mu_m |z|} \tag{35}$$

$$E_r(r_2,z) = \frac{q_1}{2\pi\epsilon_0 a^2} \sum_{m=1}^{\infty} \frac{J_0(\mu_m r_1) J_1(\mu_m r_2)\ e^{-\mu_m |z|}}{[J_1(\mu_m a)]^2} \tag{36}$$

where μ_{mo} has been replaced by μ_m.

The space charge force on a reference ring of charge q_2 and radius r_2 and located at z, due to a source ring of charge q_1 and radius r_1 and located at $z = 0$, is then given by

$$F_{21,z}(r_1,r_2,z) = q_2 E_z(r_2,z) \tag{37}$$

$$F_{21,r}(r_1,r_2,z) = q_2 E_r(r_2,z) \tag{38}$$

Equations (35) to (38) cannot be used to calculate space-charge forces because the summations will approach infinity if r_1 approaches r_2 and z approaches zero. We must take into account the nonzero axial and radial thickness of the rings. A fully general calculation can be made by integrating over both the source ring, located at $(r_1,0)$, and the reference ring, located at (r_2,z). Because of the complexity involved, it is not feasible to calculate these expressions each time the space charge force on one ring due to another is desired. Instead the radial and axial space-charge forces are calculated for an array of values of r_1, r_2, and z and stored in a table. This calculation is done once, just prior to the beginning of the simulation. In the simulation, the space-charge forces are evaluated by a three-dimensional linear interpolation on the table.

In carrying out the integrations over the axial and radial thicknesses of the rings, assumptions must be made on what these thicknesses are. It is assumed that the axial thickness, $\ell_d = \lambda_e/N_d$ (see fig. 2), remains constant. The radial thickness is determined from the assumption that the ratio of the inner radius to centroid radius and the ratio of the outer radius to centroid radius remain constant. The inner and outer radii are obtained from a given centroid radius by using equations (2) and (3). Since these radii depend on the ring type j, the space-charge force is really a function of five variables: r_1, r_2, z, j_1, j_2. Since j_1 and j_2 can take on all values from 1 to R, R^2 tables must be calculated. The storage and time requirements for calculating this many tables may be excessive for some applications. These requirements are reduced if a less general formulation is adopted. We note that when calculating the rf electric-field forces on a reference ring, the approach we take is to calculate this field and evaluate it at the centroid values of r and z of the reference ring. We can adopt the same approach with the space-charge field forces; that is, we calculate the space charge field by integrating over the axial and radial thicknesses of all source rings and then evaluate the field at the centroid values of r and z of the reference ring. Since we integrate over source rings but not reference rings, the space-charge force is now a function of four variables: r_1, r_2, z, j_1. In this approach only R tables must be calculated.

The two models for calculating space-charge forces described in the previous paragraph will be referred to as the R^2-tables model and the R-tables model. We will discuss the relative merits of the two models. But first we mention a modification that can be made to the R-tables model. The modification is to integrate over the <u>axial</u> thickness of the reference ring. This modification only slightly increases the computational complexity and does not increase the number of required tables. Also space-charge forces become smoother functions of z. To indicate the increased smoothness as a function of z, figure 4 shows the axial space-charge force on an innermost ring due to another innermost ring, as a function of z, with and without the modification just described. Another advantage of this modification is that, for cases where $r_1 = 0$, $r_2 > 0$ and $z < \ell_d$, the summation for the radial space-charge force is a convergent series, whereas this series is divergent without the modification. Also, the summations for both axial and radial forces converge more rapidly with the modification. In all further discussions of the R-tables model, it is assumed that the modification is made.

Comparison of the R^2-tables model to the R-tables model for a variety of cases shows that disagreement in the space-charge force on a reference ring due to any one source ring is less than 7 percent in practical situations. Typically there is considerably less disagreement in the space-charge force on a reference ring due to <u>all</u> source rings. Figure 5 shows a typical comparison of the R^2-tables model to the R-tables model. We consider these disagreements to be reasonably small, especially when compared to the error already present in the model from the assumption that there are no gaps in the tunnel. We therefore adopt the R-tables model because of its reduced computational and storage requirements.

The expressions for the axial and radial space-charge forces for the R-tables model are obtained by carrying out the appropriate integrations involved in equations (35) and (36). Letting $r_{1,in}$ and $r_{1,out}$ be the inner and outer radii of the source ring, we obtain

$$F_{21,z}(r_1,r_2,z) = \frac{\mathrm{sgn}(z)q_1q_2}{2\pi\epsilon_o a^2}\sum_{m=1}^{\infty}\frac{J_o(\mu_m r_2)G_a(r_{1,in},r_{1,out})G_b(z)}{[J_1(\mu_m a)]^2}$$

$$F_{21,r}(r_1,r_2,z) = \frac{q_1q_2}{2\pi\epsilon_o a^2}\sum_{m=1}^{\infty}\frac{J_1(\mu_m r_2)G_a(r_{1,in},r_{1,out})G_b(z)}{[J_1(\mu_m a)]^2} \qquad |z| > \ell_d \quad (39)$$

$$F_{21,z}(r_1,r_2,z) = \frac{\mathrm{sgn}(z)q_1q_2}{2\pi\epsilon_o a^2}\sum_{m=1}^{\infty}\frac{J_o(\mu_m r_2)G_a(r_{1,in},r_{1,out})G_c(z)}{[J_1(\mu_m a)]^2}$$

$$F_{21,r}(r_1,r_2,z) = \frac{q_1q_2}{2\pi\epsilon_o a^2}\sum_{m=1}^{\infty}\frac{J_1(\mu_m r_2)G_a(r_{1,in},r_{1,out})G_d(z)}{[J_1(\mu_m a)]^2} \qquad |z| < \ell_d \quad (40)$$

where the functions G_a, G_b, G_c, G_d are defined as

$$G_a(r_{1,in},r_{1,out}) = \frac{r_{1,out}J_1(\mu_m r_{1,out}) - r_{1,in}J_1(\mu_m r_{1,in})}{\frac{1}{2}\mu_m\left(r_{1,out}^2 - r_{1,in}^2\right)}$$

$$G_b(z) = \frac{-2e^{-\mu_m|z|} + e^{-\mu_m(|z|-\ell_d)} + e^{-\mu_m(|z|+\ell_d)}}{\mu_m^2\ell_d^2}$$

$$G_c(z) = \frac{2 - 2e^{-\mu_m|z|} - e^{\mu_m(|z|-\ell_d)} + e^{-\mu_m(|z|+\ell_d)}}{\mu_m^2\ell_d^2} \qquad (41)$$

$$G_d(z) = \frac{-2\mu_m(|z|-\ell_d) - 2e^{-\mu_m|z|} + e^{\mu_m(|z|-\ell_d)} + e^{-\mu_m(|z|+\ell_d)}}{\mu_m^2\ell_d^2}$$

For the region $r_1 = 0$, $r_2 > 0$, $z < \ell_d$, the summation for the radial space-charge force is a very slowly converging series. For this region, we use an alternate computation. We subdivide the region into two regions: (1) $r_1 = 0$, $0 < r_2 < 0.125a$, $z < \ell_d$, and (2) $r_1 = 0$, $r_2 > 0.125a$, $z < \ell_d$.

For the first region the tunnel wall is far removed from the source ring and reference ring, and we consider the rings to be in free space. For this case the radial force on a reference ring of zero axial thickness is given by

$$F_{21,r}(r_1 = 0, r_2, z) = \frac{q_1 q_2 r_2}{4\pi\varepsilon_0 \ell_d} \left\{ \frac{\left[\left(\frac{-\ell_d}{2} - z\right)^2 + r_2^2\right]^{-\frac{1}{2}}}{\left(\frac{-\ell_d}{2} - z\right) + \left[\left(\frac{-\ell_d}{2} - z\right)^2 + r_2^2\right]^{\frac{1}{2}}} - \frac{\left[\left(\frac{\ell_d}{2} - z\right)^2 + r_2^2\right]^{-\frac{1}{2}}}{\left(\frac{\ell_d}{2} - z\right) + \left[\left(\frac{\ell_d}{2} - z\right)^2 + r_2^2\right]^{\frac{1}{2}}} \right\}, \qquad 0 < r_2 < 0.125a \qquad (42)$$

The radial force on a reference ring of axial thickness ℓ_d is obtained by numerically integrating the above equation. For the second region, the presence of the tunnel wall cannot be neglected. It can be shown that

$$\frac{\partial F_{21,r}(r_1 = 0, r_2, z)}{\partial r_1} = 0$$

Thus $F_{21,r}(r_1 = 0, r_2, z)$ should differ only slightly from $F_{21,r}(r_1 = \Delta r_{sc}, r_2, z)$, where $r_1 = \Delta r_{sc}$ represents the first nonzero r_1 grid point. We use this approximation in the second region for calculating $F_{21,r}(r_1 = 0, r_2, z)$.

$$F_{21,r}(r_1 = 0, r_2, z) = F_{21,r}(r_1 = \Delta r_{sc}, r_2, z), \qquad r_2 > 0.125a \qquad (43)$$

For the region $r_1 = 0$, $r_2 = 0$, $z < \ell_d$, the summation for the axial space-charge force is a divergent series. For this case, the source and reference "rings" are actually line charges of length ℓ_d which partially overlap one another. We choose to truncate this summation after 100 terms, a somewhat arbitrary choice, and use the result for the axial force. It should be noted that the grid points in this region will be used rarely, if at all. They will be used only when a reference ring and a source ring, at the same time, have centroid radii less than Δr_{sc} and are separated axially by less than ℓ_d.

From figure 4, we have an idea of the smoothness of the axial space-charge force as a function of z. The radial force as a function of z has a similar degree of smoothness. From examining these functions we can determine the spacing between grid points in the z-direction that is required in the space-charge tables for sufficiently accurate interpolation. In figure 4, $\ell_d/a = 1/3$. The shape of these functions varies somewhat with varying values of ℓ_d/a. After examining these functions for a range of values of ℓ_d/a, we decided to use two different grid spacings. Letting Δz_{sc} be the spacing between z grid points, we use

$$\Delta z_{sc} = \frac{1}{4}\,\ell_d, \qquad 0 \le z \le 3\ell_d \tag{44}$$

$$\Delta z_{sc} = \frac{1}{2}\,\ell_d, \qquad z > 3\ell_d \tag{45}$$

Let z_{max} be the last z grid point in the space-charge tables. In the simulation, if the axial separation distance between two rings exceeds z_{max}, the space-charge forces are set to zero. We calculate z_{max} such that the error in setting these forces to zero is less than 1 percent. An empirical formula is used to obtain z_{max}.

$$\frac{z_{max}}{a} = 0.09\left[\frac{\ln\left(\frac{0.345}{\ell_d/a}\right)}{0.693}\right]^2 - 0.26\left[\frac{\ln\left(\frac{0.345}{\ell_d/a}\right)}{0.693}\right] + 2.41, \qquad \frac{\ell_d}{a} > 0.127 \tag{46}$$

$$\frac{z_{max}}{a} = 2.22, \qquad \frac{\ell_d}{a} < 0.127 \tag{47}$$

It is undesirable for z_{max} to be nearly equal to an integer multiple of ℓ_d. To avoid such an occurrence, z_{max} is increased slightly so that z/ℓ_d is equal to an integer plus 1/2. To cut down on storage requirements, we use no more than 26 z grid points. If z_{max}/ℓ_d is greater than 9 1/2, we must increase the grid spacing Δz_{sc} to satisfy the constraint of a maximum of 26 z grid points. When z_{max}/ℓ_d is greater than 9 1/2, Δz_{sc} is redefined to be

$$\Delta z_{sc} = \frac{1}{4}\,\ell_d, \qquad 0 \le z \le 3\ell_d \tag{48}$$

$$\Delta z_{sc} = \frac{z_{max} - 3\ell_d}{13}, \qquad z > 3\ell_d \tag{49}$$

We should also examine the space-charge forces as functions of either of the two r variables. We concentrate our attention on the radial force since this is the more rapidly-varying force. We consider an example of the functional dependence on r in figure 6. For this case, $R = 3$ and the source ring is a "middle" ring of inner radius 0.326a, centroid radius 0.4a, and outer radius 0.462a. Figure 6 is the radial space-charge force on a reference ring, due to the source ring, as a function of the reference ring's centroid radius. The two rings are at the same axial position. The vertical dotted lines represent the inner and outer radius of the source ring. The other dotted line represents the linear interpolation of this function for a radial grid spacing of $\Delta r_{sc} = a/N_{sc,r}$ with $N_{sc,r} = 10$. The accuracy of the interpolation is poor in the regions near $r = 0.326a$ and $r = 0.462a$. At $r = 0.462a$ the interpolation error is 27 percent. When $N_{sc,r}$ is increased to 20, this error is reduced to 12 percent. For rough-cut runs, $N_{sc,r} = 10$ may provide sufficient accuracy, but $N_{sc,r} = 20$ should be used when greater accuracy is desired. The larger value of $N_{sc,r}$ should certainly be used in cases where the average beam diameter is small compared to the tunnel diameter.

The radial space charge force becomes much more rapidly varying as either of the r variables becomes smaller. For this reason, we use a smaller grid spacing for small values of r in such a way that the total number of grid points is still $N_{sc,r} + 1$. For larger values of r, the spacing between grid points is only slightly greater than it would be for completely uniform spacing. The radial grid spacing is given by (we assume $N_{sc,r}$ is a multiple of 5)

$$\Delta r_{sc} = \frac{5a}{N_{sc,r}^2}, \qquad 0 \le r \le \frac{a}{N_{sc,r}} \tag{50}$$

$$\Delta r_{sc} = \frac{5a(N_{sc,r} - 1)}{4N_{sc,r}^2}, \qquad r > \frac{a}{N_{sc,r}} \tag{51}$$

The space charge force on a given ring may be a slowly varying function of the independent variable z. This is likely to be true in the beginning cavities of the tube. To take advantage of the slowly varying nature of the space charge force, the calculation is not done on every integration step. The calculation of space charge forces is initially done every N^{th} step, where N is an input. The value of N may change during the simulation in a manner to be described later. On those integration steps where space charge forces are not calculated, they are approximated by quadratic curve fits. Each ring has its own curve fit. These curve fits are obtained by fitting a quadratic polynomial through the latest three calculations of space charge forces. Let us say that these three calculations were done when z was equal to z_a, z_b, and z_c. At an integration step where a new space charge force calculation is due, at $z = z_d$, the values calculated are compared with those obtained when the curve fits based on the points z_a, z_b, and z_c are evaluated at z_d. If the difference in the values for any ring is exceeded by a specified tolerance, the next calculation of space charge forces occurs 1/2 N steps later. In general, N is halved each time the specified tolerance is exceeded.

For calculating space charge forces, the positions of all rings must be known at a time t. This information is not readily available since z rather than t is the independent variable. To calculate the space charge force on the i^{th} ring located at some z, we must determine the positions of all the other rings at the time $t_i(z)$. Consider the j^{th} ring. The time of arrival $t_j(z)$ at z is known. By the periodicity of the motion, the ring that originally was m wavelengths behind the j^{th} ring arrives at z at the time $t_j(z) + mT$, where T is the reciprocal of frequency. Similarly, the ring that originally was m wavelengths ahead of the j^{th} ring arrives at z at the time $t_j(z) + (-m)T$. We consider all such rings and find m such that

$$|t_i(z) - (t_j(z) + mT)| = \text{Minimum} \tag{52}$$

We may call the ring in question the j^{th} ring in the m^{th} cycle. We assume that the j^{th} ring in any other cycle is too far away from the i^{th} ring, at the time $t_i(z)$, to contribute significantly to the space charge force on the i^{th} ring. Let (r_j^m, z_k^m) be the position of the j^{th} ring in the m^{th} cycle at the time $t_i(z)$. We obtain (r_j^m, z_j^m) by assuming that this ring has constant axial velocity $v_{jz}(z)$ and constant radial velocity $v_{jr}(z)$ in the time

interval spanned by $t_i(z)$ and $t_j(z) + mT$. Then (r_j^m, z_j^m) is given by

$$r_j^m = r_j(z) + v_{jr}(z)[t_i(z) - (t_j(z) + mT)] \tag{53}$$

$$z_j^m = z + v_{jz}(z)[t_i(z) - (t_j(z) + mT)] \tag{54}$$

The space charge force is then calculated based on the reference ring radius $r_i(z)$, the source ring radius r_j^m, and the axial separation distance $z - z_j^m$. The calculation is done for all rings, excluding the i^{th} ring, and the results are summed to obtain the total space charge force on the i^{th} ring. When the axial separation distance $z - z_j^m$ is greater than z_{max} (see eqs. (46) and (47)), the space charge calculation is not done for this term in the summation.

As discussed in reference 2, relativistic corrections are applied to axial lengths. In the space-charge equations, z and ℓ_d are replaced by z' and ℓ_d' given by

$$\ell_d' = \frac{\ell_d}{\sqrt{1 - \left(\frac{\dot{z}_o}{c}\right)^2}} \tag{55}$$

$$z' = \frac{z}{\sqrt{1 - \left(\frac{\dot{z}_o}{c}\right)^2}} \tag{56}$$

Radiofrequency electric field forces. - If the complex voltage V on a given gap is known, the electric field in the neighboring region can be written in an expansion of the form

$$E_z(r,z,t) = \frac{-\mu V}{2\ell \sinh(\mu)} \sum_{m=-\infty}^{\infty} \frac{C_m I_o(\gamma_m r)}{L I_o(\gamma_m a)} e^{-i\beta_m z} e^{i\omega t} \tag{57}$$

$$E_r(r,z,t) = \frac{-\mu V}{2\ell \sinh(\mu)} \sum_{m=-\infty}^{\infty} \frac{i\beta_m C_m I_1(\gamma_m r)}{\gamma_m L I_o(\gamma_m a)} e^{-i\beta_m z} e^{i\omega t} \tag{58}$$

where

$$C_m = \frac{2\ell[\mu \sinh(\mu)\cos(\beta_m \ell) + \beta_m \ell \cosh(\mu)\sin(\beta_m \ell)]}{(\mu)^2 + (\beta_m \ell)^2} \tag{59}$$

$$\beta_m = \beta_o + \frac{2\pi m}{L} \tag{60}$$

$$\gamma_m = \sqrt{\beta_m^2 - \frac{\omega^2}{c^2}} \tag{61}$$

and $\beta_o L$ is the lowest order phase shift per cavity. The shaping factor μ is an input parameter.

We define $Q_z(r,z)$ and $Q_r(r,z)$ as

$$Q_z(r,z) = \frac{\mu}{\sinh(\mu)} \sum_{m=-\infty}^{\infty} \frac{C_m I_o(\gamma_m r)}{L I_o(\gamma_m a)} e^{-i\beta_m z} \tag{62}$$

$$Q_r(r,z) = \frac{\mu}{\sinh(\mu)} \sum_{m=-\infty}^{\infty} \frac{i\beta_m C_m I_1(\gamma_m r)}{\gamma_m L I_o(\gamma_m a)} e^{-i\beta_m z} \tag{63}$$

Equations (57) and (58) can now be written as

$$E_z(r,z,t) = \frac{-V}{2\ell} Q_z(r,z)\, e^{i\omega t} \tag{64}$$

$$E_r(r,z,t) = \frac{-V}{2\ell} Q_r(r,z)\, e^{i\omega t} \tag{65}$$

Equations (64) and (65) are appropriate to a forward-traveling circuit wave. For a combination of a forward- and backward-traveling wave, the appropriate expressions are

$$E_z(r,z,t) = \frac{-1}{2\ell} [Q_z(r,z)V_f + Q_z^*(r,z)V_b] e^{i\omega t} \tag{66}$$

$$E_r(r,z,t) = \frac{-1}{2\ell} [Q_r(r,z)V_f + Q_r^*(r,z)V_b] e^{i\omega t} \tag{67}$$

The electric-field force on a ring of charge q and located at (r,z) at time t is then given by

$$F_z = R_e \left[\frac{-q}{2\ell} (Q_z(r,z)V_f + Q_z^*(r,z)) e^{i\omega t} \right] \tag{68}$$

$$F_r = R_e \left[\frac{-q}{2\ell} (Q_r(r,z)V_f + Q_r^*(r,z)) e^{i\omega t} \right] \tag{69}$$

Many of the quantities in equations (57) to (69) change from cavity to cavity. When a particular cavity, let us say the k^{th} cavity, is being discussed, the subscript k will be appended to these quantities. We now consider the i^{th} ring in the k^{th} cavity located at the n^{th} node z_{nk}. The centroid radius

of the ring is $r_j(z_{nk})$. The electric-field force is evaluated at $r = r_j(z_{nk})$ and $z = z_{nk}$. From equations (68) and (69), the electric-field force on the ring is

$$F_{z,jnk} = R_e\left[\frac{-q_j}{2\ell_k}\left(Q_{zk}(r_j(z_{nk}),z_{nk})V_{fk} + Q^*_{zk}(r_j(z_{nk}),z_{nk})V_{bk}\right)e^{i\omega t_j(z_{nk})}\right] \tag{70}$$

$$F_{r,jnk} = R_e\left[\frac{-q_j}{2\ell_k}\left(Q_{rk}(r_j(z_{nk}),z_{nk})V_{fk} + Q^*_{rk}(r_j(z_{nk}),z_{nk})V_{bk}\right)e^{i\omega t_j(z_{nk})}\right] \tag{71}$$

The $Q_{zk}(r,z)$ and $Q_{rk}(r,z)$ functions are evaluated for an array of r and z values and stored in tables when cavity k is entered. The z values are the nodes z_{nk}, $n = 1, \ldots, N_z$. The r values are equally spaced values from $r = 0$ to $r = a$. The number of r values is an input parameter. The $Q_{zk}(r_j(z_{nk}),z_{nk})$ and $Q_{rk}(r_j(z_{nk}),z_{nk})$ in equations (70) and (71) are evaluated by doing a linear interpolation in r on these stored tables. The number of terms included in the summations for Q_{zk} and Q_{rk} is determined by an input parameter. If cavity k has the same L_k, ℓ_k, β_{ok}, μ_k as cavity $k-1$, then $Q_{z,k-1} = Q_{zk}$ and $Q_{r,k-1} = Q_{rk}$ and new tables do not have to be calculated. When new tables do have to be calculated, the old tables are no longer needed, and the new tables may occupy the same storage space as the old tables. The electric-field forces are evaluated by equations (70) and (71).

Voltage-jump electric field forces. - If a dc voltage V_J is imposed across the gap of a cavity, the resultant electric field in the cavity is given by (ref. 5)

$$E_z(r,z) = \frac{-V_J}{L}\left[1 + \sum_{m=1}^{\infty} D_m I_o(k_m r)\cos(k_m z)\right] \tag{72}$$

$$E_r(r,z) = \frac{-V_J}{L}\left[\sum_{m=1}^{\infty} D_m I_1(k_m r)\sin(k_m z)\right] \tag{73}$$

where

$$D_m = \frac{2\mu[\mu \sinh \mu \cos k_m\ell + k_m\ell \cosh \mu \sin k_m\ell]}{\sinh \mu[\mu^2 + (k_m\ell)^2]\, I_o(k_m a)} \tag{74}$$

$$k_m = \frac{2m\pi}{L} \tag{75}$$

We define $R_z(r,z)$ and $R_r(r,z)$ as

$$R_z(r,z) = 1 + \sum_{m=1}^{\infty} D_m I_o(k_m r)\cos(k_m z) \tag{76}$$

$$R_r(r,z) = \sum_{m=1}^{\infty} D_m I_1(k_m r) \sin(k_m z) \tag{77}$$

Equations (72) and (73) can now be written as

$$E_z(r,z) = \frac{-V_J R_z(r,z)}{L} \tag{78}$$

$$E_r(r,z) = \frac{-V_J R_r(r,z)}{L} \tag{79}$$

As before, when referring to the k^{th} cavity, the subscript k will be appended to those quantities which may change from cavity to cavity. We now consider the i^{th} ring in the k^{th} cavity located at the n^{th} node z_{nk}. From equations (78) and (79), the electric-field force on the ring is

$$F_{z,ink} = \frac{-q_i V_{Jk} R_{zk}(r_i(z_{nk}), z_{nk})}{L_k} \tag{80}$$

$$F_{r,ink} = \frac{-q_i V_{Jk} R_{rk}(r_i(z_{nk}), z_{nk})}{L_k} \tag{81}$$

The $R_{zk}(r,z)$ and $R_{rk}(r,z)$ functions are calculated and stored in a table and have the same features as the $Q_{zk}(r,z)$ and $Q_{rk}(r,z)$ for rf electric-field forces

Magnetic field forces. - The program provides options for simulating two types of magnetic focusing fields: (1) uniform solenoidal focusing and (2) periodic permanent magnetic (PPM) focusing.

The magnetic field for uniform solenoidal focusing is given simply by

$$B_z(r,z) = B_0 \tag{82}$$

$$B_r(r,z) = 0 \tag{83}$$

where the constant B_0 is a program input.

The second type of magnetic focusing is PPM focusing. We consider first "single period" PPM focusing. Figure 7 shows the geometry of the ring magnets which are centered along the z-axis. The gap length between magnets is 2g, the inner diameter is 2a, and the magnetic period is P. Also shown in figure 7 is the shape of the axial magnetic field at $r = a$. The origin is at the center of a gap so that B_z is an even function of z. The assumed shape of $B_z(a,z)$ in the region $|z| \leq P/2$ is

$$B_z(\bar{a},z) = B_0 \cosh \bar{\mu} z, \qquad 0 \leq |z| \leq \frac{g}{2} \tag{84}$$

$$B_z(\bar{a},z) = 0, \qquad \frac{g}{2} \le |z| \le \frac{p}{2} - g \tag{85}$$

$$B_z(\bar{a},z) = -B_o \cosh\left[\bar{\mu}\left(z - \frac{p}{2}\right)\right], \qquad \frac{p}{2} - g \le |z| \le \frac{p}{2} \tag{86}$$

where the shaping factor $\bar{\mu}$ is an input parameter.

The magnetic field can be found using a Fourier series expansion. We note that B_z is axially symmetric and satisfies LaPlace's equation, and B_r is zero at $z = \pm P/2$. The Fourier series expansion which satisfies these conditions and has the required behavior at $r = 0$ is

$$B_z(r,z) = \sum_{n=1}^{\infty} a_n I_o(k_n r) \cos(k_n z) \tag{87}$$

where k_n is given by

$$k_n = \frac{2n\pi}{P} \tag{88}$$

Using the equation div $\vec{B} = 0$, we can show that B_r is given by

$$B_r(r,z) = \sum_{n=1}^{\infty} a_n I_1(k_n r) \cos(k_n z) \tag{89}$$

The coefficients a_n can be evaluated if $B_z(r,z)$ is a known function of z at some value of r, let us say $r = r_o$. We obtain

$$a_n = \frac{2}{P I_o(k_n r_o)} \int_0^P B_z(r_o,z) \cos k_n z \, dz \tag{90}$$

If $r_o = \bar{a}$, we use the assumed field shapes given by equations (84) to (86). Substituting into equation (90), we obtain

$$\left.\begin{aligned} a_n &= \frac{8B_o[\bar{\mu} \sinh \bar{\mu}g \cos k_n g + k_n \cosh \bar{\mu}g \sin k_n g]}{P\left(\bar{\mu}^2 + k_n^2\right) I_o(k_n \bar{a})}, \qquad n \text{ odd} \\ a_n &= 0, \qquad n \text{ even} \end{aligned}\right\} \tag{91}$$

In practice, the field shapes at $r = \bar{a}$ are not precisely known and cannot be conveniently measured. Alternatively, the on-axis values $B_z(0,z)$ are conveniently measurable and can be used in equation (90), letting $r_o = 0$, to evaluate a_n. For the case of measured data, the integral in equation (90) is evaluated numerically.

"Double period" PPM focusing is treated in much the same way as "single period" PPM focusing. Figure 8 shows the geometry of the ring magnets which are centered along the z-axis. As before, the gap length between magnets is 2g, the inner diameter is 2a, and the magnetic period is P. Also shown in figure 8 is the shape of the axial magnetic field at $r = \bar{a}$. Whereas the single periodic case has its origin at the center of a gap, the double periodic case has its origin midway between two adjacent gaps. The origin is placed here in order to make B_z an even function of z. The assumed shape of $B_z(\bar{a},z)$ in the region $|z| \leq P/2$ is

$$B_z(\bar{a},z) = 0, \qquad 0 \leq |z| \leq \frac{P}{8} - g \tag{92}$$

$$B_z(\bar{a},z) = B_o \cosh\left[\bar{\mu}\left(z - \frac{P}{8}\right)\right], \qquad \frac{P}{8} - g \leq |z| \leq \frac{P}{8} + g \tag{93}$$

$$B_z(\bar{a},z) = 0, \qquad \frac{P}{8} + g \leq |z| \leq \frac{3P}{8} - g \tag{94}$$

$$B_z(\bar{a},z) = -B_o \cosh\left[\bar{\mu}\left(z - \frac{3P}{8}\right)\right], \qquad \frac{3P}{8} - g \leq |z| \leq \frac{3P}{8} + g \tag{95}$$

$$B_z(\bar{a},z) = 0, \qquad \frac{3P}{8} + g \leq |z| \leq \frac{P}{2} \tag{94}$$

In the same way as before, the magnetic field can be found using a Fourier series expansion. The results for $B_z(r,z)$ and $B_r(r,z)$ are identical to those in equations (87) to (90). If $r_o = a$, we use the assumed field shapes given by equations (92) to (96). Substituting into equation (90), we obtain

$$\left.\begin{aligned} a_n &= \frac{\left(2 \cos \frac{n\pi}{4}\right)(8B_o)[\bar{\mu} \sinh \bar{\mu}g \cos k_n g + k_n \cosh \bar{\mu}g \sin k_n g]}{P\left(\bar{\mu}^{-2} + k_n^2\right) I_o(k_n \bar{a})}, \qquad n \text{ odd} \\ a_n &= 0, \qquad n \text{ even} \end{aligned}\right\} \tag{97}$$

As before, the on-axis values $B_z(0,z)$, obtained from measured data, may be used in equation (90), letting $r_o = 0$, to evaluate a_n.

The magnetic flux $\psi(r,z)$ for both "single period" and "double period" PPM focusing is given by

$$\psi(r,z) = \sum_{n=1}^{\infty} 2\pi r \frac{a_n I_1(k_n r)}{k_n I_o(k_n \bar{a})} \cos k_n z \tag{98}$$

The magnetic flux is needed for calculating the angular velocity $\dot{\phi}$ of a ring (see eq. (22)). Knowing $\dot{\phi}$, the axial magnetic force $r\dot{\phi}B_r$ and the radial magnetic force $r\dot{\phi}B_z$ on a ring can be calculated.

As before, when referring to the k^{th} cavity, the subscript k will be appended to those quantities which may change from cavity to cavity. We now consider the i^{th} ring in the k^{th} cavity located at the n^{th} node z_{nk}. The angular velocity $\dot{\phi}_{ink}$ of the ring is

$$\dot{\phi}_{ink} = \dot{\phi}_o - \frac{q_i}{m_i} \frac{\psi_k(r_i(z_{nk}),z_{nk}) - \psi_o}{2\pi r_i(z_{nk})^2} \tag{99}$$

The axial and radial magnetic forces on the ring are

$$F_{z,ink} = q_i r_i(z_{nk}) \dot{\phi}_{ink} B_{rk}(r_i(z_{nk}),z_{nk}) \tag{100}$$

$$F_{r,ink} = -q_i r_i(z_{nk}) \dot{\phi}_{ink} B_{zk}(r_i(z_{nk}),z_{nk}) \tag{101}$$

The $B_{zk}(r,z)$, $B_{rk}(r,z)$, and $\psi_k(r,z)$ functions are calculated and stored in a table and have the same features as the $Q_{zk}(r,z)$, $Q_{rk}(r,z)$, $R_{zk}(r,z)$, and $R_{rk}(r,z)$ tables.

Rings with small radius. - In this section we discuss the behavior of rings which become very small in radius. As we shall see, a modification to the simulation will be required. It is instructive to analyze the equations of motion and obtain an approximation to the radial motion of such rings.

We look at the case of an innermost ring, which is really a disk, since this ring type is the one most likely to become very small. We use non-relativistic equations and assume the cathode flux is zero. From equation (16), the radial equation of motion is

$$\frac{d^2r}{dt^2} = \frac{q}{m}(E_{rf,r} + E_{sc,r} + r\dot{\phi}B_z) + r\dot{\phi}^2 \tag{102}$$

From equation (22), $\dot{\phi}$ is

$$\dot{\phi} = \frac{-q}{m} \frac{\psi(r,z)}{2\pi r^2} \tag{103}$$

For small r, $B_z(r,z)$ can be approximated by $B_z(0,z)$. Then $\psi(r,z)$ can be approximated by

$$\psi(r,z) = \pi r^2 B_z(0,z) \tag{104}$$

Substituting equation (104) into equation (103), we obtain

$$\dot{\phi} = \frac{-qB_z(0,z)}{2m} \tag{105}$$

Substitution of equation (105) into equation (102) yields

$$\frac{d^2r}{dt^2} = \frac{-q^2B_z^2(0,z)r}{4m^2} + \frac{q}{m}\left(E_{rf,r} + E_{sc,r}\right) \tag{106}$$

We transform the above equation to one with z as independent variable, assuming that the axial velocity v_z is constant over the region of interest.

$$\frac{d^2r}{dz^2} = \frac{-q^2B_z^2(0,z)r}{4m^2v_z^2} + \frac{q}{mv_z^2}\left(E_{rf,r} + E_{sc,r}\right) \tag{107}$$

For r small enough, the space-charge field is dominated by the self-force. We assume r is small enough that the space-charge field can be approximated by the self-force only. From Gauss' law, the self-force is closely approximated by

$$E_{sc,r} = \frac{q}{2\pi\epsilon_o\ell_d r} \tag{108}$$

Equation (107) becomes

$$\frac{d^2r}{dz^2} = \frac{-q^2B_z^2(0,z)r}{4m^2v_z^2} + \frac{q}{mv_z^2}E_{rf,r} + \left(\frac{q^2}{2\pi\epsilon_o mv_z^2\ell_d}\right)\frac{1}{r} \tag{109}$$

The first two terms on the right hand side of equation (109) are negligible compared to the third term for small enough r. We then obtain the approximation

$$\frac{d^2r}{dz^2} = \frac{K}{r} \tag{110}$$

$$K = \frac{q^2}{2\pi\epsilon_o mv_z^2\ell_d} = \frac{|q/m|I_o}{4\pi\epsilon_o u_o v_z^2} \tag{111}$$

Equation (110) cannot be solved analytically; however, we can determine the minimum value of r. For shorter notation, we use a "prime" to denote differentiation with respect to r. We consider the situation where $r(z)$ and $r'(z)$ are known at some point z_1.

$$r(z_1) = r_1$$

$$r'(z_1) = r_1'$$

We assume further that $r(z)$ is decreasing and reaches a minimum value r_2 at some point z_2. The following derivation for r_2 is self-explanatory.

$$r'' = \frac{K}{r}$$

$$2r'r'' = \frac{2Kr'}{r}$$

$$\frac{d}{dz}\left(\frac{dr}{dz}\right)^2 = \frac{2K}{r}\frac{dr}{dz}$$

$$d\left(\frac{dr}{dz}\right)^2 = 2K\frac{dr}{r}$$

$$\left(\frac{dr}{dz}\right)^2\Bigg|_1^2 = 2K \ln r\Bigg|_1^2$$

$$(r_2')^2 - (r_1')^2 = 2K \ln \frac{r_2}{r_1}$$

Continuing the derivation and noting that $r_2' = 0$, we have

$$\frac{-(r_1')^2}{2K} = \ln \frac{r_2}{r_1}$$

$$e^{-(r_1')^2/2K} = \frac{r_2}{r_1}$$

$$r_2 = r_1 e^{-(r_1')^2/2K}$$

We consider a numerical example from a computer run simulating the Communications Technology Satellite (CTS) 200-watt TWT (ref. 9). The pertinent data are:

$$r_1 = 0.05a = 0.3175\times10^{-4} \text{ m}$$

$$r_1' = \frac{-3.5}{57.3} \text{ (corresponds to 3.5° angle)}$$

$$u_o = v_z = 0.63 \times 10^8 \frac{m}{sec}$$

$$I_o = 0.07 \text{ amps}$$

With this data, we obtain for r_2/a

$$\frac{r_2}{a} = 0.73 \times 10^{-3}$$

The actual trajectory, obtained from numerical integration of equation (110), is shown in figure 9. In the neighborhood of the minimum point, r" is changing very rapidly and very small integration steps need to be taken. Since the program is designed to have a fixed number of equally-sized steps per cavity, it is not possible to accurately calculate the type of trajectory shown in figure 9, without using a prohibitively large number of steps per cavity. We notice from figure 9 that the ring approaches the z-axis so closely that it almost appears as though the ring is reflected from the axis. In the program, we simulate such a trajectory as though the ring is indeed reflected from the z-axis. Assume a ring has radius r and first derivative r' at the end of an integration step and that the step size is Δz. If the ring satisfies the following condition,

$$r + 2\Delta z\, r' < 0$$

then the decision is made that the normal integration mode will not accurately calculate the ring radius over the next step. Instead the acceleration on the ring is set to zero and the simulation proceeds. When the integration step is reached at which the ring radius would otherwise become negative, the reflection takes place and dr/dz changes sign. After the reflection takes place, the actual value of the ring acceleration is restored, and the normal mode of simulation proceeds. In figure 10 the resultant trajectory (dashed line) is compared to the actual trajectory.

Beam-Wave Coupling Analysis

The fields induced by the beam current can be conveniently represented by induced gap voltages. The analysis for obtaining expressions for the induced voltages is given in reference 5 (pp. 11-15). From equations (66) and (67), the forward and backward components of the vector electric field can be expressed as

$$\vec{E}_f(r,z,t) = \frac{-V_f}{2\ell} \vec{Q}(r,z)\, e^{i\omega t} \tag{112}$$

$$\vec{E}_b(r,z,t) = \frac{-V_b}{2\ell} \vec{Q}^*(r,z)\, e^{i\omega t} \tag{113}$$

where $\vec{Q}(r,z)$ is defined as $Q_z(r,z)\vec{a}_z + Q_r(r,z)\vec{a}_r$. Equations (46) and (47) of reference 5, when generalized to the three-dimensional case, become

$$\Delta V_f = \frac{Z}{4\ell} \int_v \vec{Q}^*(r,z) \cdot \vec{J}_1(r,z)dv \tag{114}$$

$$\Delta V_b = \frac{Z}{4\ell} \int_v \vec{Q}(r,z) \cdot \vec{J}_1(r,z)dv \tag{115}$$

where $\vec{J}_1(r,z)$ is the fundamental Fourier component of the beam current density $\vec{J}(r,z,t)$, v is the volume of the cavity in question, and Z is the cavity's interaction impedance.

Since $|Q_r(r,z)| << |Q_z(r,z)|$ and $|J_{1r}(r,z)| << |J_{1z}(r,z)|$, we may approximate $\vec{Q}(r,z) \cdot \vec{J}_1(r,z)$ by $Q_z(r,z)\, J_{1z}(r,z)$. Appendix B gives a deviation of the following expression for $J_{1z}(r,z)$

$$J_{1z}(r,z) = \frac{1}{T} \sum_{i=1}^{N_d R} \frac{g(r;r_{i,in},r_{i,out})q_i(z)}{\pi\left(r_{i,out}^2 - r_{i,in}^2\right)} \frac{\sin\left(\frac{\omega\ell_d}{2v_1(z)}\right)}{\frac{\omega\ell_d}{2v_1(z)}} e^{-i\omega t_1(z)} \tag{116}$$

In the above expression $g(r;r_{i,in},r_{i,out})$ is the rectangular function defined by

$$\begin{aligned} g(r;r_{i,in},r_{i,out}) &= 1, \quad r_{i,in} < r < r_{i,out} \\ g(r;r_{i,in},r_{i,out}) &= 0, \quad r < r_{i,in} \text{ or } r > r_{i,out} \end{aligned} \tag{117}$$

where $r_{i,in}$ and $r_{i,out}$ are the inner and outer radius of the i^{th} ring. The backward induced voltage, from equation (115), now becomes

$$\Delta V_b = \frac{Z}{4\ell} \int_v J_{1z}(r,z)Q_z(r,z)dv \tag{118}$$

Using equation (116), equation (118) becomes

$$\Delta V_b = \frac{Z}{4\ell} \int_{z=-\frac{L}{2}}^{\frac{L}{2}} \frac{1}{T} \sum_{i=1}^{N_d R} \frac{q_i(z)}{\pi\left[r_{i,out}^2(z) - r_{i,in}^2(z)\right]} \frac{\sin\left(\frac{\omega\ell_d}{2v_1(z)}\right)}{\frac{\omega\ell_d}{2v_1(z)}} e^{-i\omega t_1(z)}$$

$$\times \int_{r_{i,in}(z)}^{r_{i,out}(z)} Q_z(r,z)\, 2\pi r\, dr\, dz \qquad (119)$$

The integration in r can be shown to be

$$\int_{r_{i,in}(z)}^{r_{i,out}(z)} Q_z(r,z)\, r\, dr = \frac{\mu}{\sinh \mu} \sum_{m=-\infty}^{\infty} \frac{r C_m I_1(\gamma_m r) e^{-i\beta_m z}}{L\gamma_m I_o(\gamma_m a)} \Bigg|_{r_{i,in}(z)}^{r_{i,out}(z)} \qquad (120)$$

We define $S(r,z)$ as follows:

$$S(r,z) = \frac{\mu}{\sinh \mu} \sum_{m=-\infty}^{\infty} \frac{C_m I_1(\gamma_m r) e^{-i\beta_m z}}{L\gamma_m a I_o(\gamma_m a)} \qquad (121)$$

Equation (120) becomes

$$\int_{r_{i,in}(z)}^{r_{i,out}(z)} Q_z(r,z)\, r\, dr = a\, r_{i,out}(z)\, S(r_{i,out}(z),z) - a\, r_{i,in}(z)\, S(r_{i,in}(z),z) \qquad (122)$$

With the aid of equation (122), equation (119) becomes

$$\Delta V_b = \int_{z=-\frac{L}{2}}^{\frac{L}{2}} G_b(z)dz \qquad (123)$$

where $G_b(z)$ is given by

$$G_b(z) = \frac{Z}{4\ell} \frac{1}{T} \sum_{i=1}^{N_d R} \frac{q_i(z)}{\pi\left[r_{i,out}^2(z) - r_{i,in}^2(z)\right]} \frac{\sin \frac{\omega \ell_d}{2v_i(z)}}{\frac{\omega \ell_d}{2v_i(z)}} e^{-i\omega t_i(z)}$$

$$\times 2\pi a[r_{i,out}(z)\, S(r_{i,out}(z),z) - r_{i,in}(z)\, S(r_{i,in}(z),z)] \qquad (124)$$

Similarly, ΔV_f is given by

$$\Delta V_f = \int_{z=-\frac{L}{2}}^{\frac{L}{2}} G_f(z)\, dz \tag{125}$$

where $G_f(z)$ is given by

$$G_f(z) = \frac{Z}{4\ell}\frac{1}{T}\sum_{i=1}^{N_d R}\frac{q_i(z)}{\pi\left[r_{i,out}^2(z) - r_{i,in}^2(z)\right]}\frac{\sin\dfrac{\omega\ell_d}{2v_i(z)}}{\dfrac{\omega\ell_d}{2v_i(z)}}\, e^{-i\omega t_i(z)}$$

$$\times\, 2\pi a\left[r_{i,out}(z)\, S^*(r_{i,out}(z),z) - r_{i,in}(z)\, S^*(r_{i,in}(z),z)\right] \tag{126}$$

In equations (123) to (126), the integration variable z is the axial position relative to the center of cavity k. To avoid excessively cumbersome notation, the subscript k has been omitted from these equations. The integrals in equations (123) and (125) are evaluated with the use of Simpson's rule with end corrections. The end corrections were derived with the assumption that the number of nodes per cavity N_z is a multiple of four. Equations (123) and (125), with the subscript k restored, now become

$$\Delta V_{fk} = \Delta z_k \sum_{n=1}^{N_z} \delta_n G_f(z_{nk}) \tag{127}$$

$$\Delta V_{bk} = \Delta z_k \sum_{n=1}^{N_z} \delta_n G_b(z_{nk}) \tag{128}$$

where, from Simpson's rule with end corrections, the δ_n are

$$\left.\begin{aligned} &\delta_1 = \frac{1}{3} + \frac{17}{24} && \delta_n = \frac{2}{3},\ 4 \le n \le N_z - 2,\ \text{if } n \text{ is odd} \\ &\delta_2 = \frac{4}{3} - \frac{7}{24} && \delta_n = \frac{4}{3},\ 4 \le n \le N_z - 2,\ \text{if } n \text{ is even} \\ &\delta_3 = \frac{2}{3} + \frac{2}{24} && \delta_{N_z-1} = \frac{1}{3} + \frac{9}{24} \\ & && \delta_{N_z} = \frac{27}{24} \end{aligned}\right\} \tag{129}$$

From equations (124) and (126), the evaluation of $G_f(z_{nk})$ and $G_b(z_{nk})$ requires the evaluation of $S_k(r_{i,out}(z_{nk}),z_{nk})$ and $S_k(r_{i,in}(z_{nk}),z_{nk})$ for $i = 1, \ldots, N_dR$. The $S_k(r,z)$ function is calculated and stored in a table in the same manner and with the same features as the $R_{zk}(r,z)$, $R_{rk}(r,z)$, $Q_{zk}(r,z)$ and $Q_{rk}(r,z)$ tables. The evaluation of $S_k(r,z)$ in equations (124) and (126) is done by linearly interpolating the table in the r variable.

Calculating the effects of the backward wave requires an iterative procedure. In the first pass through the tube, the ΔV_{bk} are calculated and stored for each cavity k. From the ΔV_{bk}, the backward voltages for a cavity chain from cavity $k1$ to cavity $k2$ are obtained from

$$V_{b,k2} = \Delta V_{b,k2} \tag{130}$$

$$V_{bk} = \Delta V_{bk} + V_{b,k+1} \sqrt{\frac{Z_k}{Z_{k+1}}}\, e^{-(\alpha L)_{bk}}\, e^{-i(\beta_1 L)_k}, \qquad k = k2 - 1, \ldots, k1 \tag{131}$$

By a cavity chain, we mean a sequence of consecutive cavities whose backward voltages are to be calculated. After V_{bk} are known for the desired cavities, a second pass is made through the tube. The second pass yields a new set of ΔV_{bk} that can be used for calculating a set of V_{bk} for a third pass. The process continues until convergence is obtained. In many applications the iterative procedure will converge faster if the iteration is done on one cavity chain at a time. This would be true, for example, for a tube having severs. The program has the capability of performing the iterative procedure for an arbitrary set of cavity chains.

The computational procedure in the beam-wave interaction process is as follows:

(1) When cavity k is entered, calculate and store the $S_k(r,z)$ table given by equation (121). If cavity k has the same L_k, ℓ_k, β_{0k}, μ_k as cavity $k-1$, then $S_{k-1}(r,z) = S_k(r,z)$ and a new table does not have to be calculated.

(2) Obtain a first approximation to ΔV_{fk} by assuming that the rings have constant axial and radial velocities in cavity k. Thus

$$\left.\begin{aligned} t_i(z_{nk}) &= t_i(z_{1k}) + \frac{dt(z_{1k})}{dz}(z_{nk} - z_{1k}) \\ r_i(z_{nk}) &= r_i(z_{1k}) + \frac{dr(z_{1k})}{dz}(z_{nk} - z_{1k}) \end{aligned}\right\} \qquad n = 1, \ldots, N_z \tag{132}$$

Knowing $r_i(z_{nk})$, we can readily calculate $r_{i,out}(z_{nk})$ and $r_{i,in}(z_{nk})$. Knowing $t_i(z_{nk})$, $r_{i,out}(z_{nk})$ and $r_{i,in}(z_{nk})$, we can calculate the first approximation to ΔV_{fk} from equations (126), (127) and (129).

(3) Let the forward voltage for cavity k be

$$V_{fk} = \sqrt{\frac{Z_k}{Z_{k-1}}}\, V_{f,k-1}\, e^{-(\alpha L)_{f,k-1}}\, e^{-i(\beta_1 L)_{k-1}} + \Delta V_{fk}$$

If there is a backward voltage, we assume it is known from equation (131) using the set of ΔV_{bk} obtained from the previous pass through the tube.

(4) Proceed with numerical integration of the equations of motion to obtain trajectory data at each node and antinode in the cavity.

(5) At the n^{th} node in the cavity, after $t_i(z_{nk})$ and $r_i(z_{nk})$ have been obtained, calculate and store $\delta_n G_f(z_{nk})$ and $\delta_n G_b(z_{nk})$. These quantities are the n^{th} terms in the summations of equations (127) and (128).

(6) When the last integration step in cavity k has been done, calculate a better approximation to ΔV_{fk} from equation (127). The ΔV_{fk} so obtained replaces the old ΔV_{fk} calculated in step 2. Also, calculate ΔV_{bk} from equation (128). The ΔV_{bk} are stored for use in the next pass through the tube.

(7) If additional accuracy is required, make another pass through the cavity, repeating steps 3 to 6.

(8) Repeat steps 1 to 7 for cavity $k + 1$.

(9) When the last cavity is done and the effects of the backward wave have to be determined, make a second pass through the tube. The backward voltages for the second pass are determined from the ΔV_{bk} of the first pass.

(10) Make as many passes through the tube as are required to obtain convergence.

Summary of Program Steps

The entire computational procedure is given in flow chart form in figure 11. The procedure is summarized by the following steps:

(1) Read input data.

(2) Calculate the tables for space charge forces.

(3) Begin numerical integration of equations of motion with z as the independent variable.

(4) When a new cavity is entered, let us say the k^{th} cavity, print data for cavity $k - 1$. If the parameters of cavity k are different from those of cavity $k - 1$, calculate the tables that are required for evaluation of rf forces, voltage-jump forces, magnetic forces, and induced voltages. Obtain a first approximation to ΔV_{fk} by assuming that the rings have constant velocity throughout cavity k. Attenuate and phase shift $V_{f,k-1}$ and vectorially add the result to ΔV_{fk} to obtain the forward voltage for cavity k.

(5) When the last integration step in cavity k has been done, calculate a better approximation to ΔV_{fk}, and use the new approximation in place of the old. Also, calculate and store ΔV_{bk}.

(6) If additional accuracy is required, make a second pass through cavity k.

(7) Repeat from step 4 for cavity $k + 1$.

(8) If the effects of the backward wave are to be determined, make a second pass through the tube.

(9) Make as many passes through the tube as are required to obtain convergence.

DESCRIPTION OF INPUT DATA

The following data are required by the program. In the following definitions, a "magnetic section" is defined to be one-half of the magnetic period

for single-period PPM focusing and is defined to be one-fourth of the magnetic period for double-period PPM focusing.

Name	Symbol	Description
ACM	a	Tunnel radius, cm
ALPHL(K)	$(\alpha L)_{fk}$	Voltage attenuation of forward wave in going from cavity K to cavity K + 1, dB per cavity; K = 1, LASTCV
ALPHLR(K)	$(\alpha L)_{bk}$	Voltage attenuation of backward wave in going from cavity K + 1 to cavity K, dB per cavity; K = 1, LASTCV. (ALPHLR needs to be loaded only if KLOSS = 1.)
BO(K)	B_{ok}	Value of axial magnetic field $B_z(r,z)$ at r = a and z = midpoint of gap in K^{th} magnetic section; webers per square meter; K = 1, LASTMG. Note that r = a corresponds to the boundary value of r, and that a is also the tunnel radius. BO(K) needs to be loaded only if NBZDAT = 0.
BTLDP(K)	$\frac{(\beta_1 L)_k}{\pi}$	Phase shift of voltage for cavity K; K = 1, LASTCV.
BCM(I)	b	I^{th} beam radius in one-dimensional region, cm; I = 1, NUMB. See NUMB, NB1, NB2 for related inputs. If there is no one-dimensional region (KAV13 = INITCV), only BCM(1) is used and BCM(1) is initial beam radius.
BZDATA(I)		Experimentally obtained value of $B_z(r,z)$ at r = 0 and z = I^{th} axial data point; I = 1, NBZDAT + 1. I = 1 corresponds to the beginning of a magnetic section and I = NBZDAT + 1 corresponds to the end of a magnetic section. The axial data points must be equally spaced. BZDATA(I) needs to be loaded only if NBZDAT ≠ 0.
DRDZ(I)	$\frac{dr}{dz}$	Initial value of dr/dz for I^{th} ring; I = 1, NRINGS. I = 1 corresponds to an innermost ring. I = NRINGS corresponds to an outermost ring.
FREQGH	f	Frequency, GHz
IOBMA	I_o	Beam current at tube entrance, mA
INITCV		Number of first cavity considered in the present case
ISAVE		ISAVE = I1 + I2 + I3, where I1, I2, and I3 are defined as follows: I1 = 0: No action. I1 = 1: Initial state of the present case will be stored in COMMON/STATE/for use in a future case. I2 = 0: No action I2 = 2: Initial state of the present case will be stored in a specified data set. I3 = 0: No action. I3 = 4: Final state of the present case will be stored in a specified data set.
ISTATE		Used only when INITCV ≠ 1: ISTATE = 1: Initial state of present case is equal to initial state of previous case. ISTATE = 2: Initial state of present case is equal to final state of previous case. ISTATE = 3: Initial state of present case is equal to initial state of the last case for which I1 (see ISAVE) was equal to 1. ISTATE = 4: Initial state of present case is equal to the state stored in a specified data set.

JSCF	Initially, space charge forces are evaluated once every JSCF steps.
KAV13	Number of the first cavity in the three-dimensional region
KIMP	KIMP = 0: Pierce impedance is entered as input. KIMP = 1: Total impedance is entered as input. (See ZIMP for related input.)
KLMAG	KLMAG = 0: Cavity lengths and magnetic sections coincide. KLMAG ≠ 0: Cavity lengths and magnetic sections do not coincide.
KLOSS	KLOSS = 0: ALPHLR(K) will be set equal to ALPHL(K); thus, ALPHLR(K) does not need to be loaded.
KPLOT	KPLOT = 0: Plots are desired. KPLOT ≠ 0: Plots are not desired.
KPPM	KPPM = 1: Single period PPM focusing is to be used. KPPM = 2: Double period PPM focusing is to be used.
KPRINT	KPRINT = 0: Print input data. KPRINT ≠ 0: Do not print input data.
KREL	KREL = 0: Use relativistic equations of motion. KREL ≠ 0: Use nonrelativistic equations of motion.
KSMSIG	KSMSIG = 0: Print small-signal parameters. KSMSIG ≠ 0: Do not print small-signal parameters.
KSPACE	KSPACE = 0: Calculate space charge forces. KSPACE ≠ 0: Set space charge forces equal to zero.
KSOLEN	KSOLEN = 0: Use PPM focusing. KSOLEN ≠ 0: Use solenoidal focusing; B_z = B0, B_r = 0.
KVEL(I)	Number of cavity for the I^{th} printout of normalized axial velocities of rings; I = 1, NVEL
KWRITM	KWRITM = 0: Do not print normalized masses of rings. KWRITM ≠ 0: Print normalized masses of rings whenever normalized axial velocities of rings are printed.
KWRITV	KWRITV = 0: Do not print normalized radial velocities of rings. KWRITV ≠ 0: Print normalized radial velocities of rings, v_r/u_o, whenever normalized axial velocities of rings are printed.
LASTCV	Number of last cavity considered in the present case (LASTCV ≤ 70)
LASTMG	Number of magnetic sections (LASTMG ≤ 70)
LCIRCM(K)	Length of K^{th} cavity, cm; K = 1, LASTCV.
LGAPCM(K)	Length of gap in K^{th} cavity, cm; K = 1, LASTCV.
LMAGCM(K)	Length of K^{th} magnetic section, cm; K = 1, LASTMG. LMAGCM(K) needs to be loaded only if KLMAG ≠ 0.
MSHAPE(K)	Used in defining electric field shape for K^{th} cavity, inverse meters; K = 1, LASTCV;

$$\frac{E_z(a,z) \text{ at gap edge}}{E_z(a,z) \text{ at gap center}} = \cosh(m\ell)$$

where m = MSHAPE(K) and ℓ = half-length in meters of K^{th} gap.

MU(K)	μ	Used in defining magnetic field shape for K^{th} magnetic section, inverse meters; K = 1, LASTMG; $\frac{B_z(a,z) \text{ at gap edge}}{B_z(a,z) \text{ at gap center}} = \cosh(\mu g)$ where μ = MU(K) and g = half-length in meters of K^{th} magnetic gap. MU(K) needs to be loaded only if NBZDAT = 0.
NB1		Used only when there is a one-dimensional region (KAV13 > INITCV). Beam radius changes from first value to second value at end of $NB1^{th}$ cavity. (NB1 needs to be loaded only if NUMB > 1.)
NB2		Used only when there is a one-dimensional region (KAV13 > INITCV). Beam radius changes from second value to third value at end of $NB2^{th}$ cavity. (NB2 needs to be loaded only if NUMB = 3.)
NBWM		NBWM = 0: No backward wave. NBWM > 0: Number of last cavity considered in calculating backward wave.
NBZDAT		NBZDAT = 0: Magnetic fields are determined by input data BØ and MU. NBZDAT ≠ 0: Magnetic fields are determined from experimental data. The number of experimental data values for $B_z(0,z)$ is NBZDAT + 1. (NBZDAT ≤ 100)
NCAVSS		Number of cavity for which small-signal parameters are calculated
NDISKS	N_d	Number of disks (NDISKS ≤ 24)
NMAX		For sums that are stored in tables, excluding space-charge force tables and magnetic field tables, NMAX is the upper limit. (NMAX ≤ 50)
NPGRID	N_r	Number of grid points in r direction is NPGRID + 1. r = 0 is first grid point and r = a is last grid point. Refers only to the grid for calculating forces on rings due to electric and magnetic fields. (NPGRID ≤ 20)
NPSC	$N_{sc,r}$	Number of grid points in r direction is NPSC + 1. r = 0 is first grid point and r = a is last grid point. Refers only to grid for calculating forces on rings due to space-charge fields. (NPSC ≤ 20)
NRINGS	R	Number of rings per disk (NRINGS ≤ 4)
NUMB		Number of discrete values for the beam diameter in the one-dimensional region. 1 ≤ NUMB ≤ 3
NVEL		Number of cavities for which ring axial velocities are to be printed out.
NXGRD1	N_z	Number of nodes in z-direction per cavity, in one-dimensional region. (NXGRD1 ≤ 64); NXGRD1 must be a multiple of 4.
NXGRD3	N_z	Number of nodes in z-direction per cavity, in three-dimensional region. (NXGRD3 ≤ 64); NXGRD3 must be a multiple of 4.
NXMAG		Number of grid points in z-direction per magnetic section. NXMAG must be a multiple of 4. Normally, NXMAG should be about the same as NXGRD3. NXMAG does not have to be loaded if KLMAG = 0. (NXMAG ≤ 64)

PCDPA	ψ_c/ψ_a	Normalized cathode flux: PCDPA = ψ_c/ψ_a, where ψ_c is cathode flux at r = a. $\psi_a = \pi a^2 B_0$, where a is tunnel radius and $B_0 \equiv$ BO(1).
PINDBM		Input power, dBm
TOLDV		Error criterion for determining whether an additional pass through a cavity is required. If $$\frac{\Delta V_{f,new} - \Delta V_{f,old}}{V_{f,new}} > \text{TOLDV}$$ then an additional pass is made.
TOLSC		Error criterion for determining whether the frequency of calculating space charge forces should be doubled. If for any ring the difference between the calculated space charge force and the extrapolation of the quadratic curve fit is greater than the product of TOLSC and the maximum rf electric field force in the cavity, the frequency of calculating space charge forces is doubled.
TOLTBL		Error criterion used in electric and magnetic field tables for determining the number of terms to include in infinite summations. Suggested value: TOLTBL = 0.02.
TWOGCM(K)	2g	Length of gap in K^{th} magnetic section, cm; K = 1, LASTMG
VØB	V_0	Beam voltage, volts
VJUMP(K)	V_{Jk}	The dc voltage jump for K^{th} cavity, volts; K = 1, LASTCV
ZIMP(K)	Z_k	If KIMP = 0, ZIMP(K) is the Pierce impedence in ohms for K^{th} cavity; K = 1, LASTCV If KIMP = 1, ZIMP(K) is the total impedance in ohms for K^{th} cavity; K = 1, LASTCV

DESCRIPTION OF OUTPUT DATA

The program output consists of both printed output and plots. The plots are produced only if the input parameter KPLOT is zero. The printed output includes three parts: (1) printing of small-signal parameters (only if the input parameter KSMSIG is zero); (2) a cavity-by-cavity printing of selected data; (3) printing of data on ring dynamics at selected cavities. The program can be easily modified to calculate and print other data if desired.

First, the input data are printed in NAMELIST format. (The printing of the input data can be suppressed by letting KPRINT be nonzero.) Then the small-signal parameters are printed if desired. The small-signal parameters are as follows:

Name	Symbol	Description
UO	u_0	Initial beam velocity, m/sec
BEB	$\beta_e b$	Product of beam propagation constant and beam radius
BIB	$\beta_i b$	Product of wave propagation constant and beam radius
KP	K_p	Pierce impedance, ohms
ZC	Z_c	Total impedance, ohms
C	C	Pierce's C
B	b	Pierce's b
D	d	Pierce loss parameter d

DGAIN		**Asymptotic gain per cavity, dB/cavity**
QQ	Q	Pierce's space charge parameter, QC/C
A1PA2	$A_1 + A_2$	Launching loss, dB

The following data are printed for each cavity:

CAV		Cavity number
VMAG		Magnitude of gap voltage, volts
ISMAG		Magnitude of normalized induced current
ISPHA		Phase of normalized induced current divided by π
LSGAIN		Large-signal gain, dB
POUT		Output power divided by I_0V_0
AVERHO	$\bar{\rho}$	Average of the ring radii $\bar{\rho} = \frac{1}{NR}\sum_{i=1}^{NR} \rho_i$ (NR = NDISKS*NRPD)
RMSANG		RMS value of the angle that the velocity vectors of the rings make with the z-axis; in degrees

$$\text{RMSANG} = \sqrt{\frac{1}{NR}\sum_{i=1}^{NR}\left(\frac{d\rho_i}{d\xi}\right)^2} \cdot \frac{180}{\pi}$$

RMSVEL — RMS value of the normalized radial velocities of the rings, where the normalization is with respect to u_0, the initial axial velocity

$$\text{RMSVEL} = \sqrt{\frac{1}{NR}\sum_{i=1}^{NR}\left(\frac{dr}{dt}\frac{}{u_0}\right)^2}$$

PKE	Change in beam kinetic power referred to initial beam kinetic power, divided by I_0V_0
INTRC	Power loss due to beam interception, divided by I_0V_0
PRF	Power in forward wave, divided by I_0V_0
PBW	Power in backward wave, divided by I_0V_0
PLC	Cumulative power loss (except for loss due to beam interception), divided by I_0V_0
PBAL	Power balance equal to

$$1 + \frac{PKE - PJUMP + PRF + PBW + PLC + INTRC}{I_0V_0}$$

where PJUMP is the power due to all voltage jumps up to the current cavity

SC	Integer variable KSCF: space charge forces are evaluated every KSCF integration steps.

At selected cavities, the following data are printed:

"Normalized axial velocities" - Axial velocities normalized with respect to u_0, the initial axial velocity

"Normalized radial velocities" - Radial velocities normalized with respect to u_0, the initial axial velocity; printed only if KWRITV $\neq$ 0

"Normalized ring masses" - Ring masses normalized with respect to initial ring mass; printed only if KWRITM $\neq$ 0

"Ring radius divided by a" - Ring radii normalized with respect to a

DESCRIPTION OF GLOBAL VARIABLES

Global variables are variables that are used by more than one subroutine and hence are put into COMMON blocks. In the following descriptions, we exclude input data variables since these have already been described.

Name	Symbol	Description
DELV(K)	ΔV_{fk}	Forward induced voltage for k^{th} cavity, volts; K = 1, LASTCV
DELVR(K)	ΔV_{bk}	Backward induced voltage for k^{th} cavity, volts; K = 1, LASTCV
DVTEMP(K)	ΔV_{fk}	Approximate forward induced voltage for k^{th} cavity, obtained by assuming rings have constant axial and radial velocities throughout cavity, volts; K = 1, LASTCV
DVRTEM(K)	ΔV_{bk}	Backward induced voltage of previous case, for k^{th} cavity, volts; K = 1, LASTCV
VGAP(K)	V_k	Sum of forward voltage and backward voltage for k^{th} cavity, volts; K = 1, LASTCV
VGAPF(K)	V_{fk}	Forward voltage for k^{th} cavity, volts; K = 1, LASTCV
VGAPR(K)	V_{bk}	Backward voltage for k^{th} cavity, volts; K = 1, LASTCV
A	a	Tunnel radius, meters
ALF1(J,I)		Ratio of inner radius to mean radius of $(J,I)^{th}$ ring, I = 1, NDISKS; J = 1, NRINGS
ALF2(J,I)		Ratio of outer radius to mean radius of $(J,I)^{th}$ ring, I = 1, NDISKS; J = 1, NRINGS
ALF1Ø(J)		Initial ratio of inner radius to mean radius of a ring, where J = 1 is an innermost ring and J = NRINGS is an outermost ring
ALF2Ø(J)		Initial ratio of outer radius to mean radius of a ring, where J = 1 is an innermost ring and J = NRINGS is an outermost ring
ALPHLB(K)	$(\alpha L)_{bk}$	Voltage attenuation of backward wave in going from cavity K + 1 to cavity K, dB per cavity; K = 1, LASTCV
B(I)	b	I^{th} beam radius in one-dimensional region, meters; I = 1, NUMB

BSUBR(IR,IZ)	$B_r(r_{IR},z_{IZ})$	Radial component of focusing magnetic field at grid point (r_{IR},z_{IZ}), webers per square meter; IR = 1, NPGRID + 1, IZ = 1, NXMAG. Calculated in TBL3M and MAGCF.
BSUBZ(IR,IZ)	$B_z(r_{IR},z_{IZ})$	Axial component of focusing magnetic field at grid point (r_{IR},z_{IZ}), webers per square meter; IR = 1, NPGRID + 1, IZ = 1, NXMAG. Calculated in TBL3M and MAGCF.
C	c	Speed of light, meters per second
C1(I)		Constant associated with I^{th} beam diameter; I = 1, NUMB. Calculated in INDAT.
C2(I)		Constant associated with I^{th} beam diameter; I = 1, NUMB. Calculated in INDAT.
C3		Constant calculated in INDAT.
CAVFLG		Flag used by subroutine KSCKC to determine which of two adjacent cavities is to be selected when positioned at the boundary between the two cavities
CNORM	$c/\omega a$	Normalized speed of light
CONST1		Constant calculated in INDAT
CONST2		No longer used
CONST4		Constant calculated in INDAT
COSY(K)		Array of cosine values used in TBL3E; K = 1, 2 * NXGRID + 1. Calculated in INDAT.
COSYB(K)		Array of cosine values used in TBL3M; K = 1, 4 * KPPM * NXMAG + 1. Calculated in INDAT.
CTHETA	$\cos\theta$	Cosine of normalized time
DELP	$\Delta\rho$	Normalized distance between two adjacent grid points in radial direction. Calculated in INDAT.
DELPSC(I)		I^{th} normalized distance between two adjacent grid points in radial direction in space charge tables; I = 1, 2. Calculated in SCAT3.
DELX(I)	$\Delta\xi$	Integration step size in I^{th} cavity string; I = 1, NSCAV. Calculated in INDAT.
DELXSC(I)		I^{th} normalized distance between two adjacent grid points in axial direction in space charge tables; I = 1, 2. Calculated in SCAT3.
DPR		Conversion factor from degrees to radians, DPR = $180/\pi$
ECHARG	e	Charge of an electron, coulomb; ECHARG is positive
EMASS		Mass of an electron, kg
EPSØ	ϵ_o	Permittivity of free space, farad/meter
ERRWT(I,J)		Error weights used in determining the number of terms to include in the summations calculated in TBL3E and TBL3M; I = 1, 5; J = 1, NPGRID + 1. Calculated in INDAT.
FREQ	f	Frequency, Hz
IØB	I_o	Beam current at tube entrance, amps

IØBAVE		Beam current at tube entrance, reduced by the percentage of the beam that has been intercepted, at the present axial position, amps. Calculated in ACC.
INTLS		Power loss due to the cumulative beam interception that has taken place up to the present axial position, watts
ISCAV(K)		Number of cavity string in which K^{th} cavity is located; K = 1, LASTCV
ITER		Present number of iteration of beam rings traversing cavity
KBEGIN		Equals zero at beginning of case and is set equal to 1 immediately thereafter.
KCAV		Number of current cavity
KOUNTP		Counter for data points to be plotted
KPDZC(K)	K_p/Z	Ratio of Pierce impendence to total impedance for K^{th} cavity; K = 1, LASTCV
KSCAV		Number of present cavity string. (A cavity string is a string of consecutive cavities all having the same geometrical and electrical properties.)
KSCF		Space charge forces are calculated every KSCF steps.
KSCFT		Used to store a previous value of KSCF.
KSTOP		Equals zero until end of last cavity, when it is set equal to 1.
KX		Number of current node, counted from first node of first cavity
KXØ		Initial node of present case, counted from first node of first cavity
KXPRI		Number of current node, counted from first node of current cavity
KXSC		Number of node, counted from first node of first cavity, at which the most recent calculation of space charge forces was done
LAMB	λ	Beam wavelength, meters
LCIR(K)	L_k	Length of K^{th} cavity, meters; K = 1, LASTCV
LDISK	ℓ_d	Axial length of a ring, meters
LDISKN	ℓ_d/a	Normalized axial length of a ring
LMAG(K)		Length of K^{th} magnetic section, meters; K = 1, LASTMG
LSMALL(K)	ℓ_k	One-half of gap length in K^{th} cavity, meters; K = 1, LASTCV
MDISK	m_d	Mass of a disk at tube entrance, kg
MLSHML	$\frac{m\ell}{\sinh m\ell}$	$m\ell$ is the product of MU and LSMALL for the current cavity
MRINGØ		Mass of a ring at tube entrance, kg
MRING(J,I)		Mass of $(J,I)^{th}$ ring, kg; I = 1, NDISKS; J = 1, NRINGS
MUA(I)		I^{th} zero of Bessel function J_0; I = 1 100
MUØ	μ_o	Permeability of free space, henry/meter
NB		Number of current beam-diameter region. (A beam-diameter region is a region throughout which the beam diameter is constant.) Applies only to one-dimensional region.

NCAVPS(I)		Number of cavities in I^{th} cavity string; I = 1, NSCAV
NCASE		Number of current case
NCUMCS(I)		Number of last cavity in I^{th} cavity string; I = 1, NSCAV
NPSC1		Number of grid points in the first of two radial grids in space-charge tables
NR		Total number of rings in a beam wavelength (NDISKS * NRPD)
NRPD		Number of rings per disk (NRPD = 1 in one-dimensional region.)
NSCAV		Total number of cavity strings
NXGRID		Number of nodes in z-direction per cavity
NXISC		Number of grid points in the axial grid in space-charge tables
POB	ρ_0	I_0/u_0, charge density per unit length at tube entrance, coulomb/m
PBW(K)		Power in backward wave in K^{th} cavity, watts; K = 1, LASTCV. Calculated in ENBAL.
PHIDN(J,I)	ϕ_{ji}/ω	Normalized angular velocity of $(J-I)^{th}$ ring; I = 1, NDISKS; J = 1, NRINGS. Calculated in FACC3.
PI	π	3.141593
PKE(K)		Kinetic power at end of K^{th} cavity minus kinetic power at beginning of tube, watts; K = 1, LASTCV. Calculated in ENBAL.
PLC		Cumulative power loss at end of K^{th} cavity, watts; K = 1, LASTCV. Calculated in ENBAL.
POBAL		Power balance. Calculated in ENBAL.
PRF(K)		Power in forward wave in K^{th} cavity, watts; K = 1, LASTCV. Calculated in ENBAL.
PRICL		Power in backward wave in present cavity, watts. Same as PBW(K). Calculated in ENBAL.
PSI(IR,IZ)	$\psi(r_{IR},z_{IZ})$	Magnetic flux at grid point (r_{IR},z_{IZ}), webers; IR = 1, NPGRID + 1, IZ = 1, NXMAG. Calculated in TBL3M and MAGCF.
PSIA	$\pi a^2 B_0$	Normalizing factor. Calculated in INDAT.
PSC1(J,I) PSC2(J,I) PSC3(J,I)		Radial space charge force on $(J,I)^{th}$ ring at each of the latest 3 selected values of independent variable ξ used for quadratic curve-fitting; J = 1, NRINGS; I = 1, NDISKS. Calculated in SCFT3.
PSCA(J,I) PSCB(J,I) PSCC(J,I)		Coefficients of the quadratic polynomial used for curve-fitting the radial space charge force on $(J,I)^{th}$ ring; J = 1, NRINGS; I = 1, NDISKS. Calculated in SCFT3.
QDISK	q_d	Charge of a disk at tube entrance, coulombs
QRINGO		Charge of a ring at tube entrance, coulombs
QRING(J,I)		Charge of $(J-I)^{th}$ ring, coulomb; I = 1, NDISKS; J = 1, NRINGS
RELC(J,I)	$\sqrt{1 - \frac{v_{ji}^2}{c^2}}$	Relativistic correction factor for $(J-I)^{th}$ ring; I = 1, NDISKS; J = 1, NRINGS. Calculated in FACC3.

RHOØ(J)	ρ_{0j}	Initial value of normalized mean radius of a ring, where J = 1 is an innermost ring and J = NRINGS is an outermost ring; J = 1, NRINGS. Calculated in INDAT.
RHOMAX		Normalized outer radius of the outermost ring at the current value of ξ. Calculated in ACC.
RHO(J,I)	ρ_{ji}	Normalized radius of $(J-I)^{th}$ ring; I = 1, NDISKS; J = 1, NRINGS. Calculated in XINT.
RHOP(J,I)	$\frac{d\rho_{ji}}{d\xi}$	First derivative of ρ_{ji} with respect to ξ; I = 1, NDISKS, J = 1, NRINGS. Calculated in XINT.
RHOPP(J,I)	$\frac{d^2\rho_{ji}}{d\xi^2}$	Second derivative of ρ_{ji} with respect to ξ; I = 1, NDISKS, J = 1, NRINGS. Calculated in ACC.
SBETØA(I)	$\beta_0 a$	Value of $\beta_0 a$ for cavities in I^{th} cavity string; I = 1, NSCAV
SCA1(I) SCA2(I) SCA3(I)		I^{th} entry in table of space charge forces for first, second, and third beam diameters; I = 1, NXISC + 1. Calculated in SCAT1. Applies to one-dimensional region only.
SCHOLD		No longer used.
SIMPS(I)	δ_i	I^{th} coefficient for Simpson's rule integration; I = 1, NXGRID. Calculated in INDAT.
SINY(K)		Array of sine values used in TBL3E; K = 1, 2 * NXGRID + 1. Calculated in INDAT.
SINYB(K)		Array of sine values used in TBL3M; K = 1, 4 * KPPM*NXMAG + 1. Calculated in INDAT.
SLCIR(I)		Length of cavities in I^{th} cavity string, meters; I = 1, NSCAV
SLSMAL(I)		One-half of gap length for cavities in I^{th} cavity string, meters; I = 1, NSCAV
SMSHAP(I)		Electric field shaping factor for cavities in I^{th} cavity string, meters; I = 1, NSCAV
SR1MB2	$\sqrt{1 - \left(\frac{u_0}{c}\right)^2}$	Relativistic correction factor. Calculated in INDAT.
SSGAIN(K)		Small-signal gain at K^{th} cavity, based on small-signal calculations using geometrical and electrical properties of cavity number NCAVSS; K = 1, LASTCV. Calculated in SMSIG.
STHETA	$\sin\theta$	Sine of normalized time
THT(J,I)	θ_{ji}	Value of normalized time of arrival of $(J-I)^{th}$ ring at current axial position ξ; I = 1, NDISKS; J = 1, NRINGS. Calculated in XINT.
THTP(J,I)	$\frac{d\theta_{ji}}{d\xi}$	First derivative of θ_{ji} with respect to ξ; I = 1, NDISKS; J = 1, NRINGS. Calculated in XINT.

THTPP(J,I)	$\frac{d^2\theta_{ji}}{d\xi^2}$	Second derivative of θ_{ji} with respect to ξ; I = 1, NDISKS: J = 1, NRINGS. Calculated in ACC.
THTPLT(J,I)		Value of θ for $(J,I)^{th}$ ring used in plots; I = 1, NDISKS; J = 1, NRINGS
TPXR(IR,IZ,L) TPXI(IR,IZ,L)		Real (TPXR) and imaginary (TPXI) components of the L^{th} table for the data point (r_{IR}, z_{IZ}); IR = 1, NPGRID + 1; IZ = 1, NXGRID: L = 1, 5 for TPXR: L = 1, 3 for TPXI. Calculated in TBL3E.
TXR(IZ,L) TXI(IZ,L)		Real (TXR) and imaginary (TXI) components of the L^{th} table for the data point z_{IZ}; IZ = 1, NXGRID; L = 1, 3 for TXR: L = 1, 2 for TXI. Calculated in TABL1. Used for one-dimensional region only.
TWOG(K)	2g	Gap length of K^{th} magnetic section; meters; K = 1, LASTMG
TWOPI	2π	2π
UØB	u_o	Initial axial beam velocity, m/sec
UØNORM	u_o/ω_a	Normalized initial axial beam velocity
VØBSUM(K)		Beam voltage plus sum of all voltage jumps up to K^{th} cavity, volts; K = 1, LASTCV
VGAP1M		Voltage across first gap, volts
VMAX		The maximum |VGAP(K)|, where the maximum is taken over all values of K up to the present cavity; volts. Calculated in BTWNC.
W	ω	Radian frequency, $\omega = 2\pi f$; rad/sec
X	ξ	Current value of normalized position along tube axis, measured from beginning of first cavity
XØ	ξ_o	Initial value of normalized position along tube axis for the present case, measured from beginning of first cavity
XICAV(K)		Normalized axial position at end of K^{th} cavity; K = 1, LASTCV
XIMAG(K)		Normalized axial position at end of K^{th} magnetic section; K = 1, LASTMG
XISCAV(I)		Normalized axial position at end of I^{th} cavity string; I = 1, NSCAV
XIMXSC		Maximum normalized axial separation distance in space charge force tables. (If two rings are separated by a distance greater than XIMXSC, the space charge force on one ring due to the other is set to zero.) Calculated in INDAT.
XISC1 XISC2 XISC3		The three latest values of ξ at which space charge forces were calculated
XPRI		Present value of normalized position along tube axis, measured from beginning of current cavity. Calculated in ACC.
XSC1(J,I) XSC2(J,I)		Axial space charge force on $(J,I)^{th}$ ring at each of the latest 3 selected values of in-

XSC3(J,I)		dependent variable ξ used for quadratic curve-fitting; J = 1, NRINGS, I = 1, NDISKS. Calculated in SCFT3.
XSCA(J,I) XSCB(J,I) XSCC(J,I)		Coefficients of the quadratic polynomial used for curve-fitting the axial space charge force on $(J-I)^{th}$ ring; J = 1, NRINGS; I = 1, NDISKS. Calculated in SCFT3.
ZC(K)		Total impedance for K^{th} cavity, ohms; K = 1, LASTCV
IOTABL(K) I1TABL(K)	$I_0(x_k)$ $I_1(x_k)$	Tables of Bessel functions I_0 and I_1, starting with $x_1 = 0$ and with an increment of 0.03 in x; K = 1,5667
SCAP(IP1,IP2,IX,II) SCAX(IP1,IP2,IX,II)		Tables of radial (SCAP) and axial (SCAX) space charge forces for three-dimensional region; IP1 = 1, NPSC + 1; IP2 = 1, NPSC + 1; IX = 1, NXISC + 1; II = 1, NRINGS. Calculated in SCAT3.

DESCRIPTION OF SUBROUTINES

In this section, the COMMON blocks, the main program, and each subroutine are described. Flow charts are included for the more complex subroutines.

COMMON Blocks

The program has five COMMON blocks. COMMON/INDATA/ contains the input data. COMMON/MREAL/ contains real and integer global variables. COMMON/MCOMP/ contains complex global variables. COMMON/PLOT/ contains arrays used for plotting Applegate diagrams. COMMON/STATE/ contains arrays used for storing initial states and final states. An initial state is a collection of variables whose values are those at the beginning of the first cavity in the tube section under consideration. A final state is the same collection of variables but whose values are those at the end of the last cavity in the tube section. The variables in this collection are those whose values must be known in order to start the simulation of a tube section. It is necessary to store these initial and final states because they may be used in later cases. For example, in simulating the second tube section, we use the final state of the first tube section as a startup.

Main Program

The main program reads the first 100 zeros of the Bessel function J_0. Subroutines STDAT, INDAT, and SMSIG are then called. When the last integration step has been done, the final state is stored in COMMON/STATE/. Depending on the value of ISTATE, the final state may also be stored in a data set for possible use in a future case. The main program calls XINT to integrate one step and calls BTWNS to check on what action should be taken between steps.

Subroutine ACC

Subroutine ACC is called by subroutine XINT. Subroutine ACC first checks to see if a new space-charge calculation is required. A new calculation is required if the last calculation was KSCF steps ago or if the current value of ξ is at a boundary between two beam-diameter regions. If a new calculation is required, then either subroutine SCFT1 or SCFT3 is called. Next, subroutine ACC calculates the normalized axial and radial accelerations of each ring. In the one-dimensional mode this calculation is done in the same way as in the one-dimensional computer program (ref. 4). In the three-dimensional mode, the accelerations result from the following forces: space-charge forces, rf electric-field forces, voltage-jump forces, magnetic forces, centripetal forces, and forces due to relativistic effects. The space-charge forces are calculated by quadratic curve fits, and the other forces are obtained by a call to subroutine FACC3. Subroutine ACC also calculates THTPP(J,I) and RHOPP(J,I), the second derivatives of the functions $\theta_{ij}(\xi)$ and $\rho_{ij}(\xi)$, respectively.

Subroutine APPLE

Subroutine APPLE is called by the main program at the end of the simulation. Subroutine APPLE manipulates plot data that has been stored in the course of the simulation and calls the plotting device for plotting r - z plots and, optionally, t - z plots.

Subroutine BTOS

Subroutine BTOS is called by subroutine INDAT and by the main program. When called by INDAT, subroutine BTOS stores in COMMON/STATE/ the collection of variables making up the initial state. When called by the main program, subroutine BTOS stores in COMMON/STATE/ the collection of variables making up the final state.

Subroutine BTWNC

Subroutine BTWNC is called by subroutine BTWNS when the end of a cavity is reached. Subroutine BTWNC determines whether another pass through the cavity is required. A second pass is not required if either of two conditions is met: (1) a second pass has already been made, or (2) the induced forward voltage is sufficiently close to the approximation of the induced forward voltage obtained by assuming constant ring velocities throughout the cavity.

If a second pass is not required, the subroutine sets up for entrance into the new cavity. If needed, new tables are calculated by calling the appropriate subroutines. Since a second pass through the new cavity may be needed, it is necessary to store the state at the beginning of the new cavity. Subroutine FSAPP is called to calculate DVTEMP, the approximation to the induced forward voltage for the new cavity. The new forward voltage is then calculated by phase shifting and attenuating the old forward voltage and adding DVTEMP. If the old cavity was the last cavity in the one-dimensional region and the new cavity is the first cavity in the three-dimensional region, subroutine TRN13 is called.

Subroutine BTWNS

Subroutine BTWNS is called by MAIN. Subroutine BTWNS determines what action should be taken between integration steps. First, subroutine INTRC is called to check on beam interception. Next, the subroutine determines whether the end of a cavity has been reached. If so, subroutine BTWNC is called. If the end of a magnetic section has been reached, subroutine TBL3M is called. Finally, the subroutine determines whether subroutine PLOTS should be called. Subroutine PLOTS is called only in the three-dimensional region.

Subroutine CAVP

Subroutine CAVP is called by subroutine INDAT. Subroutine CAVP calculates quantities related to cavities and cavity strings. A cavity string is a string of consecutive cavities all having the same electrical and geometrical properties. The number of cavities cannot exceed 70, and the number of cavity strings cannot exceed 35.

Subroutine CKPDZ

Subroutine CKPDZ is called by subroutine INDAT. Subroutine CKPDZ calculates KPDZC(K), the ratio of Pierce impedance to total impedance, for the K^{th} cavity.

Subroutine CROOT

Subroutine CROOT is called by subroutine SMSIG. Subroutine CROOT calculates the roots of the quartic polynomial involved in calculating small-signal parameters. The subroutine first solves for the roots of the cubic polynomial using the Newton-Raphson method. Using these roots as the first iterates, the subroutine then uses the Newton-Raphson method to solve for the roots of the quartic polynomial.

Subroutine DVSUM

Subroutine DVSUM is called by subroutine XINT. In the three-dimensional region, DVSUM is also called by subroutine FSAPP. Subroutine DVSUM calculates one term in the summation for the induced forward voltage, DELV, and one term in the summation for the induced backward voltage, DELVR. These terms are added to the running sums for DELV and DELVR. The summations are those given in equations (16) and (17).

Subroutine ENBAL

Subroutine ENBAL is called by subroutine BTWNC. Subroutine ENBAL calculates the power balance at the end of the cavity in question. There are six terms in the power balance: PKE, PJUMP, PRF, PBW, PLC, and INTLS. PKE is the kinetic power minus the initial kinetic power. PJUMP is the power due to all voltage jumps up to the cavity in question. PRF is the power in the forward

wave minus the power in the forward wave in the first cavity. PBW is the power in the backward wave in the first cavity minus the power in the backward wave. PLC is the sum of power losses up to the present cavity. INTLS is the power loss due to beam interception. Power balance is equal to one plus the sum of these six terms divided by the initial beam power.

Subroutine FACC1

Subroutine FACC1 is called by subroutine ACC when the simulation is in the one-dimensional mode. Subroutine FACC1 calculates EXACC, the normalized acceleration of a ring due to rf electric-field force and voltage-jump force.

Subroutine FACC3

Subroutine FACC3 is called by subroutine ACC when the simulation is in the three-dimensional mode. Subroutine FACC3 calculates EXACC and EPACC, the normalized axial and radial accelerations of a ring due to rf electric-field force and voltage-jump force. The subroutine then calculates MXACC and MPACC, the normalized axial and radial accelerations due to magnetic focusing force. The normalized centripetal acceleration, CENTRP, is then calculated. Finally, the subroutine calculates RXACC and RPACC, the normalized axial and radial accelerations due to relativistic effects.

Subroutine FIELD

Subroutine FIELD is called by subroutine FACC3 when the simulation is in the three-dimensional mode. Subroutine FIELD calculates EXRO, EXIO, EPRO, EPIO, BXO, BPO, PSIO, EXDCV, and EPDCV. EXRO and EXIO are the real and imaginary parts of the shaping factor for the axial electric field. EPRO and EPIO are the real and imaginary parts of the shaping factor for the radial electric field. BXO, BPO, and PSIO are the shaping factors for the axial magnetic field, radial magnetic field, and magnetic flux field, respectively. EXDCV and EPDCV are the shaping factors for the axial and radial voltage-jump fields.

Subroutine FSAPP

Subroutine FSAPP is called by subroutine BTWNC. Subroutine FSAPP calculates an approximation, DVTEMP, to the induced forward voltage by assuming the rings have constant axial and radial velocities in the cavity under consideration.

Subroutine INDAT

Subroutine INDAT is called by the main program. The subroutine first reads input data from a prestored data set. It then reads data entered at the terminal in NAMELIST format. Only input data that differ from those in the prestored data set need to be entered. The input data are stored in a data set for possible future use. The subroutine then calculates constants and

initializes variables. The initial state is obtained in one of three ways: (1) if the input parameter ISTATE is 4, the initial state is read from a data set; (2) if ISTATE is not 4 and INITCV (initial cavity) is 1, subroutine INIT is called and the initial state is calculated from input data; (3) if ISTATE is not 4 and INITCV is not 1, subroutine STOB is called and the initial state is obtained from COMMON/STATE/. There is storage allotment for three states in COMMON/STATE/. Which of the three is chosen is determined by ISTATE (see definition of ISTATE in the section on description of input data).

After the initial state is obtained, it is stored in COMMON/STATE/ in the first of the three storage allotments. This is done because the initial state of the present case may be used as the initial state in the following case, and thus it must be stored. The initial state is also stored in the third of the three storage allotments if the input parameter ISAVE is an odd integer. This is done because the initial state of the present case may also be required as the initial state in some future case after the following case, and thus it must be stored.

The input parameter ISAVE is the sum of I1, I2, and I3 (see definition of ISAVE in the section on description of input data). If I2 is 2, the initial state of the present case is stored in a specific data set for possible use in a future case.

If INITCV is 1, subroutine INDAT calculates the forward voltage for the first cavity. If INITCV is not 1, the forward voltage for the cavity previous to cavity INITCV is required for startup. This voltage will be known either from the previous case or by reading it from a data set. The backward voltages are calculated next. Finally, the induced backward voltages DELVR are stored in the array DVTREM. This is done because in the equations of motion we must use the induced backward voltages of the previous case. We cannot use the DELVR array because this array changes during the simulation as the new induced backward voltages are calculated. We therefore use the DVRTEM array in the equations of motion.

Subroutine INIT

Subroutine INIT is called by subroutine INDAT and only when INITCV (initial cavity) is 1. Subroutine INIT calculates initial values for the collection of variables making up the initial state.

Subroutine INTRC

At the end of each integration step, subroutine BTWNS calls subroutine INTRC to check for beam interception. The check is done for each ring. One of four conditions may occur: (1) both the inner and the outer radius of the ring are less than a, (2) the outer radius is greater than a and the inner radius is less than a, (3) both the inner and the outer radius are greater than a, (4) the ring has already been completely intercepted.

If condition (1) occurs, no action is taken. If condition (2) occurs, the outer radius is redefined to be a, and the portion of the ring located beyond $r = a$ is assumed to be intercepted. The remaining partial ring, since

its outer radius has been redefined, has a redefined value of centroid radius given by

$$r = \sqrt{\frac{r_{in}^2 + r_{out}^2}{2}}$$

The mass and charge of the ring are reduced by the appropriate amounts. The power lost due to the interception is calculated and added to the running total. If condition (3) occurs, the ring is assumed to be completely intercepted. Instead of setting the mass and charge of the ring to zero, it is more convenient to set these quantities to negligible amounts and keep the ring in the simulation. If condition (4) occurs, the outer radius of the intercepted ring is set to a, and the inner radius is set to a quantity slightly less than a.

Subroutine MAGCF

Subroutine MAGCF is called by subroutine TBL3M. In subroutine TBL3M, the arrays BSUBZB, BSUBRB, and PSIB are calculated prior to calling subroutine MAGCF. These arrays correspond to the magnetic quantities B_z, B_r, and ψ evaluated at the grid points of the magentic section in question. The axial grid points are equally spaced over the length of the magnetic section. If each magnetic section does not coincide with a cavity, these axial grid points will not coincide with the integration nodes. The program requires that the axial grid points for the B_z, B_r, and ψ tables coincide with the integration nodes. Subroutine MAGCF calculates these tables by performing linear interpolations on the BSUBZB, BSUBRB, and PSIB arrays. The results are stored in the BSUBZ, BSUBR, and PSI arrays.

Subroutine NBEAM

Subroutine NBEAM is called by subroutines BTWNC and SCFTI. When the simulation is in the one-dimensional mode, subroutine NBEAM calculates the number of the beam-diameter region in which XXX is located.

Subroutine OUTPT

Subroutine OUTPT is called by subroutine BTWNC. Subroutine OUTPT calculates and prints output data. Since the output data have already been described in another section, we will not repeat the description here.

Subroutine PLOTS

Subroutine PLOTS is called by subroutine BTWNS at each grid point z for which plotting information is to be stored. Two types of plots are used: r as a function of z and t as a function of z, for each ring to be plotted. The latter type of plot, which is similar to the Applegate diagram, is optional. The values of z, r, and t for the rings in question are stored in arrays for later usage by the plotting device.

Subroutine SACC1

Subroutine SACC1 is called by subroutine SCFT1 (one-dimensional mode only). Subroutine SACC1 calculates the space-charge acceleration of one ring due to another by linear interpolation on space-charge force tables. Although we use the term space-charge force tables, these tables actually evaluate accelerations rather than forces. If the two rings are in two different beam-diameter regions, two linear interpolations are done and the average is taken.

Subroutine SACC3

Subroutine SACC3 is called by subroutine SCFT3 (three-dimensional mode only). Subroutine SACC3 calculates the axial and radial space-charge acceleration on one ring due to another by a three-dimensional linear interpolation on space-charge force tables. Although we use the term space-charge force tables, these tables actually evaluate accelerations rather than forces.

Subroutine SCAT1

Subroutine SCAT1 is called by subroutine INDAT or subroutine INIT. For each beam diameter IB and for the I^{th} separation distance X, subroutine SCAT1 calculates the space-charge acceleration SCATMP(I,IB) of one disk due to another for the one-dimensional mode. Using EQUIVALENCE statements, we put SCA1, SCA2, and SCA3 into COMMON/MREAL/ instead of SCATMP. The arrays SCA1, SCA2, and SCA3 make up the space-charge force tables for the one-dimensional mode. In this subroutine, X is used as the separation distance between disks. Since X is also used as a global variable (current value of ξ), it is necessary to save the global variable in XSAVE. At the end of the subroutine, the value of the global variable is returned to X. In addition, subroutine SCAT1 calculates the ratio of the largest space-charge acceleration to the smallest. The smallest space-charge acceleration occurs when the separation distance is largest. Subroutine SCAT1 also calculates the ratio of the beam wavelength to the maximum separation distance.

Subroutine SCAT3

Subroutine SCAT3 is called by subroutine INDAT or subroutine INIT. For the three-dimensional mode, subroutine SCAT3 calculates and stores in a table the axial and radial space-charge accelerations of one reference ring due to one source ring. The table is three-dimensional since these accelerations are functions of three variables: (1) r_1, the centroid radius of the source ring; (2) r_2, the centroid radius of the reference ring; (3) z, the axial separation between the rings. This subroutine first calculates the number of z grid points and the spacing between z grid points. There are two different grid spacings for z (DELXSC(I), I = 1, 2). Similarly the subroutine calculates two different grid spacings for the r variables (DELPSC(I), I = 1, 2). The subroutine proceeds to calculate the space-charge accelerations for every grid point. In addition, subroutine SCAT3 calculates the ratio of the largest space-charge acceleration to the smallest. The smallest space-charge acceleration occurs when the axial separation distance is largest. Subroutine SCAT3 also calculates the ratio of the beam wavelength to the maximum separation distance.

Subroutine SCFT1

Subroutine SCFT1 is called by subroutine ACC whenever a new calculation of space-charge accelerations in the one-dimensional mode is required. Subroutine SCFT1 first calculates what the space-charge accelerations would be if the present curve fits are used. Then for each disk the subroutine calculates the space-charge acceleration of the disk by summing the accelerations due to all the other disks. The acceleration of one disk due to another is obtained by linear interpolation on the space-charge force tables. The coefficients of the new quadratic curve fits are then calculated. Finally, the subroutine determines whether the frequency of the space-charge calculation should be changed. This is done by comparing the space-charge accelerations based on the old curve fits with those just calculated. If the difference for any disk is greater than the product of TOLSC and the maximum acceleration due to the rf electric field in the cavity, the frequency of calculating space-charge accelerations is doubled.

Subroutine SCFT3

Subroutine SCFT3 is called by subroutine ACC and in some cases by subroutines INIT and TRN13. Subroutine SCFT3 is called whenever a new calculation of space-charge accelerations in the three-dimensional mode is required. This subroutine first calculates what the space-charge accelerations would be if the present curve fits are used. Then for each ring the subroutine calculates the space-charge acceleration of the ring by summing the accelerations due to all the other rings. The acceleration of one ring due to another is obtained by three-dimensional linear interpolation on the space-charge force tables. The coefficients of the new quadratic curve fits are then calculated. Finally, the subroutine determines whether the frequency of the space-charge calculation should be changed. This is done by comparing the space-charge accelerations based on the old curve fits with those just calculated. If the difference for any ring is greater than the product of TOLSC and the maximum acceleration due to the rf electric field in the cavity, the frequency of calculating space-charge accelerations is doubled.

Subroutine SMSIG

Subroutine SMSIG is called by the main program. Subroutine SMSIG calculates small-signal parameters as given in reference 7. This subroutine is identical to the one in the one-dimensional program described in reference 1. A detailed description of the subroutine is given in that reference.

Subroutine STDAT

Subroutine STDAT is called by the main program. Subroutine STDAT calculates standard data, that is, constants whose values are independent of input data.

Subroutine STOB

Subroutine STOB is called by subroutine INDAT when the initial cavity (INITCV) is not one and when the initial state is not read from a dataset. Subroutine STOB obtains the initial state from COMMON/STATE/.

Subroutine TABL1

Subroutine TABL1 is called in the one-dimensional mode by subroutine BTWNC when a new cavity is entered and tables have to be computed for the new cavity. If the new cavity has the same properties as the old cavity, subroutine TABL1 is not called. This subroutine is essentially the same as subroutine TABLE in the one-dimensional program described in reference 4. A detailed description of this subroutine is given in that reference.

Subroutine TBL3E

Subroutine TBL3E is called in the three-dimensional mode by subroutine BTWNC when a new cavity is entered. Subroutine TBL3E computes tables for electric-field shapes and voltage-jump shapes. Also computed are the tables needed to calculate induced voltages. If the new cavity has the same properties as the old cavity, new tables are not required and subroutine TBL3E makes a return to subroutine BTWNC.

Subroutine TBL3E calculates the following tables:

TPXR(j,n,1)
TPXI(j,n,1) Real and imaginary parts of the table $Q_z(r_j,z_n)$ for the shaping factor of the axial electric field. See equation (62) for the definition of $Q_z(r_j,z_n)$.

TPXR(j,n,3)
TPXI(j,n,3) Real and imaginary parts of the table $Q_r(r_j,z_n)$ for the shaping factor of the radial electric field. See equation (63) for the definition of $Q_r(r_j,z_n)$.

TPXR(j,n,2)
TPXI(j,n,2) Real and imaginary parts of the table $S(r_j,z_n)$ used in calculating induced voltages. See equation (121) for the definition of $S(r_j,z_n)$.

TPXR(j,n,4) Table $R_z(r_j,z_n)$ for the shaping factor of the axial voltage-jump field. See equation (76) for the definition of $R_z(r_j,z_n)$.

TPXR(j,n,5) Table $R_r(r_j,z_n)$ for the shaping factor of the radial voltage-jump field. See equation (77) for the definition of $R_r(r_j,z_n)$.

Subroutine TBL3M

Subroutine TBL3M is used in the three-dimensional mode only. This subroutine is called by subroutine BTWNC when a new cavity is entered and is called by subroutine BTWNS when a new magnetic section is entered. For single period PPM focusing, a magnetic section is defined to be one-half of the magnetic period. For double period PPM focusing, a magnetic section is defined to be one-fourth of the magnetic period.

Subroutine TBL3M calculates the following tables:

BSUBZB(j,n)	Axial magnetic field B_z at the grid point (r_j, z_n)
BSUBRB(j,n)	Radial magnetic field B_r at the grid point (r_j, z_n)
PSIB(j,n)	Magnetic flux field ψ at the grid point (r_j, z_n)

The axial grid points are equally spaced over the length of the magnetic section. If each magnetic section does not coincide with a cavity, these axial grid points will not coincide with the integration nodes. Subroutine MAGCF is called to obtain B_z, B_r, and ψ at the integration nodes.

Subroutine TRN13

Subroutine TRN13 is called by subroutine BTWNC when the transition from the one-dimensional mode to the three-dimensional mode is made. Subroutine TRN13 recalulates all those variables whose values change as a result of this transition.

Subroutine XINT

Subroutine XINT is called by the main program. Subroutine XINT integrates the equations of motion over one step. The numerical integration method is described in the section on the dynamics of beam rings.

CONCLUDING REMARKS

The use of the coupled-cavity traveling wave tube for space communications had led to an increased interest in improving the efficiency of the basic interaction process in these devices through velocity resynchronization and other methods. In order to analyze these methods, we have recently developed a flexible, three-dimensional, axially-symmetric, large-signal computer program for use on the IBM 370 time-sharing system. The present report is a users' manual for this program. The report describes the program in sufficient detail to allow a user to make modifications in the program if desired.

APPENDIX A

SYMBOLS

a	tunnel radius
$\bar{a}$	inner diameter of ring magnet
a_n	n^{th} Fourier coefficient in expansion for magnetic field
B_o	magnitude of axial magnetic field at $r = a$ and $z =$ middle of gap
B_r	radial component of magnetic field
B_z	axial component of magnetic field
b	initial beam radius
c	velocity of light
g	half-length of magnetic gap
I_s	modified Bessel function of order s
$J_{1z}(r,z)$	fundamental Fourier component of the beam current density
J_s	Bessel function of order s
L_k	length of k^{th} cavity
ℓ_d	axial thickness of a ring
ℓ_k	half-length of k^{th} gap
m	mass of a ring
N_c	number of cavities
N_d	number of disks per beam wavelength
N_z	number of nodes per cavity
P	magnetic period
$Q_z(r,z)$	table for calculation of rf electric field forces
$Q_r(r,z)$	table for calculation of rf electric field forces
q	charge of a ring
R	number of rings per disk
$R_z(r,z)$	table for calculation of voltage-jump forces
$R_r(r,z)$	table for calculation of voltage-jump forces
$r(z)$	centroid radius of a ring at axial location z
r_{in}	inner radius of a ring
r_{out}	outer radius of a ring
Δr_{sc}	radial grid spacing for space charge tables
$S_k(r,z)$	table for calculation of induced voltages
$t(z)$	time of arrival of a ring at axial location z
T	reciprocal of frequency

u_o	initial beam velocity
V_o	beam voltage
V_k	gap voltage, k^{th} cavity
V_{bk}	backward voltage, k^{th} cavity
V_{fk}	forward voltage, k^{th} cavity
ΔV_{bk}	backward induced voltage, k^{th} cavity
ΔV_{fk}	forward induced voltage, k^{th} cavity
Z_k	interaction impedance for k^{th} cavity
$\dot{z}$	axial velocity of a ring
Δz_{sc}	axial grid spacing for space charge tables
Δz_k	integration step size in k^{th} cavity
z_{nk}	axial position, relative to beginning of first cavity, of n^{th} node in k^{th} cavity
$(\alpha L)_{bk}$	loss factor for backward voltage in k^{th} cavity
$(\alpha L)_{fk}$	loss factor for forward voltage in k^{th} cavity
β_m	propagation factor, defined in equation (60)
$(\beta_1 L)_k$	phase shift of voltage for k^{th} cavity
ϵ_o	permittivity of free space
$\theta(\xi)$	normalized time of arrival of a ring at normalized axial location ξ
λ_e	beam wavelength
μ	shaping parameter for electric field
$\bar{\mu}$	shaping factor for magnetic field
ξ	normalized axial position; independent variable for equations of motion
$\rho(\xi)$	normalized centroid radius of a ring at normalized axial location ξ
$\sigma(z)$	charge density of a ring at axial location z
$\dot{\phi}$	angular velocity of a ring
ψ	magnetic flux
ω	angular frequency

APPENDIX B

DERIVATION OF FOURIER COMPONENT OF BEAM CURRENT DENSITY

In a previous section, the fundamental Fourier component of the beam current density was defined as

$$J_{1z}(r,z) = \frac{1}{T} \int_{t-T}^{t} J_z(r,z,t')e^{-i\omega t'} \, dt' \tag{B-1}$$

We proceed to obtain an expression for $J_{1z}(r,z)$ which is convenient for computation. The following analysis is a simple generalization of the one-dimensional analysis given in appendix B of reference 5. Let $t_i^m(z)$ be the time of arrival at z of the i^{th} ring in the m^{th} radiofrequency cycle. We let $m = 0$ for the radiofrequency cycle considered in the program. To conform with previous notation, we will henceforth omit the 0 subscript when referring to the cycle considered in the program; that is, $t_i^0(z) = t_i(z)$. Then for any integer m,

$$t_i^m(z) = t_i(z) - mT \tag{B-2}$$

In the following discussion we will use the rectangular function $g(x; x_1,x_2)$ defined as

$$\begin{aligned} g(x; x_1,x_2) &= 1, \qquad x_1 \le x \le x_2 \\ g(x; x_1,x_2) &= 0, \qquad x < x_1 \text{ or } x > x_2 \end{aligned} \tag{B-3}$$

Now consider $J_z(r,z,t)$ as a function of t for some fixed r and z (see fig. 12). We can visualize this as an observer at (r,z), observing rings as they pass by. At $t = t_i^m(z)$, the value of $J_z(r,z,t)$ is $\sigma_i(z)v_{iz}(z)g(r; r_{i,in},r_{i,out})$, where $\sigma_i(z)$ is the charge density of the i^{th} ring, $v_{iz}(z)$ is the axial velocity of the i^{th} ring, and $r_{i,in}$ and $r_{i,out}$ are the inner and outer radius of the i^{th} ring. Furthermore, $J_z(r,z,t)$ has this value for a time interval centered about $t_i^m(z)$, where the length of the interval is $\ell_d/v_{iz}(z)$. We can express this partial contribution to $J_z(r,z,t)$ as

$$\sigma_i(z)v_{iz}(z)g(r; r_{i,in},r_{i,out})g\left(t; t_i^m(z) - \frac{\ell_d}{2v_{iz}(z)}, t_i^m(z) + \frac{\ell_d}{2v_{iz}(z)}\right) \tag{B-4}$$

The total contribution to $J_z(r,z,t)$ is obtained by summing over all rings and cycles.

$$J_z(r,z,t) = \sum_{i=1}^{N_d R} \sum_{m=-\infty}^{\infty} \sigma_i(z) v_{iz}(z) g(r;\, r_{i,in}, r_{i,out})$$

$$\times\, g\left(t;\, t_i^m(z) - \frac{\ell_d}{2v_{iz}(z)},\, t_i^m(z) + \frac{\ell_d}{2v_{iz}(z)}\right) \qquad \text{(B-5)}$$

We the have for $J_{1z}(r,z)$

$$J_{1z}(r,z) = \frac{1}{T} \sum_{i=1}^{N_d R} \sum_{m=-\infty}^{\infty} \sigma_i(z) v_{iz}(z) g(r;\, r_{i,in}, r_{i,out})$$

$$\times \int_{t-T}^{t} e^{-i\omega t'}\, g\left(t';\, t_i^m(z) - \frac{\ell_d}{2v_{iz}(z)},\, t_i^m(z) + \frac{\ell_d}{2v_{iz}(z)}\right) dt' \qquad \text{(B-6)}$$

By the periodicty of the motion, there will be $N_d R$ rings passing the position z in the time interval from $t-T$ to t. In general, the $N_d R$ rings do not all come from the same rf cycle. Let m_i be the cycle number of the i^{th} ring. From equations (B-2) and (B-6), we obtain

$$J_{1z}(r,z) = \frac{1}{T} \sum_{i=1}^{N_d R} \sigma_i(z) v_{iz}(z) g(r;\, r_{i,in}, r_{i,out}) \int_{t_{i1}}^{t_{i2}} e^{-i\omega t'}\, dt' \qquad \text{(B-7)}$$

where t_{i1} and t_{i2} are given by

$$t_{i1} = t_i(z) - m_i T - \frac{\ell_d}{2v_{iz}(z)} \qquad \text{(B-8)}$$

$$t_{i2} = t_i(z) - m_i T + \frac{\ell_d}{2v_{iz}(z)} \qquad \text{(B-9)}$$

Evaluating the integral in equation (B-7) yields

$$J_{1z}(r,z) = \frac{1}{T} \sum_{i=1}^{N_d R} \sigma_i(z) \ell_d g(r;\, r_{i,in}, r_{i,out}) \frac{\sin\left(\frac{\omega \ell_d}{2v_{iz}(z)}\right)}{\frac{\omega \ell_d}{2v_{iz}(z)}} \times e^{-i\omega[t_i(z) - m_i T]}$$

(B-10)

Since $\omega m_i T = 2\pi m_i$, we have

$$J_{1z}(r,z) = \frac{1}{T} \sum_{i=1}^{N_d R} \sigma_i(z) \ell_d g(r;\, r_{i,in}, r_{i,out}) \frac{\sin\left(\frac{\omega \ell_d}{2v_{iz}(z)}\right)}{\frac{\omega \ell_d}{2v_{iz}(z)}} \times e^{-i\omega t_i(z)} \tag{B-11}$$

The charge density $\sigma_i(z)$ is given by

$$\sigma_i(z) = \frac{q_i(z)}{\pi\left(r_{i,out}^2 - r_{i,in}^2\right)\ell_d} \tag{B-12}$$

where $q_i(z)$ is the charge of the i^{th} ring. Combining equations (B-11) and
(B-12) yields

$$J_{1z}(r,z) = \frac{1}{T} \sum_{i=1}^{N_d R} \frac{g(r;\, r_{i,in}, r_{i,out}) q_i(z)}{\pi\left(r_{i,out}^2 - r_{i,in}^2\right)} \frac{\sin\left(\frac{\omega \ell_d}{2v_{iz}(z)}\right)}{\frac{\omega \ell_d}{2v_{iz}(z)}} e^{-i\omega t_i(z)} \tag{B-13}$$

REFERENCES

1. Dayton, Jr., James. A.; Kosmahl, Henry. G.; Ramins, Peter; and Stankiewicz, Norbert: Experimental Verification of a Computational Procedure for the Design of TWT-Refocuser-MDC Systems. IEEE Trans. Electron Devices, vol. ED-28, No. 12, Dec. 1981, pp. 1480-1489.
2. Kosmahl, Henry G.; and Ramins, P.: Small Size 81- and 83.5 Percent Efficient 2- and 4-Stage Depressed Collectors for Octave-Bandwidth High-Performance TWT's. IEEE Trans. Electron Devices, vol. ED-24, Jan. 1977, pp. 36-44.
3. Stankiewicz, N.: Analysis of Spent Beam Refocusing to Achieve Optimum Collector Efficiency. IEEE Trans. Electron Devices, vol. ED-24, Jan. 1977, pp. 32-36.
4. O'Malley, Thomas A.; and Connolly, Denis J.: Users' Manual for Computer Program for One-Dimensional Analysis of Coupled-Cavity Traveling Wave Tubes. NASA TM X-3565.
5. Connolly, Denis J.; and O'Malley, Thomas A.: Computer Program for Analysis of Coupled-Cavity Traveling-Wave Tubes. NASA TN D-8492.
6. Connolly, D. J.; and O'Malley, T. A.: A Contribution to Computer Analysis of Coupled-Cavity Traveling Wave Tubes. IEEE Trans. Electron Devices, volume ED-24, No. 1, Jan. 1977, pp. 27-31.
7. Kino, G. S.; et al.: Small-Signal and Large-Signal Theories for the Coupled Cavity TWT. Proceedings of the Sixth International Conference on Microwave and Optical Generation and Amplification. Inst. Electr. Eng., 1966, pp. 49-53.
8. Tien, P. K.; Walker, L. R.; and Wolontis, V. M.: A Large Signal Theory of Traveling-Wave Amplifiers. Proc. IRE, vol. 43, no. 3, Mar. 1955, pp. 260-277.
9. Kosmahl, Henry G.; McNary, B. D.; and Sauseng, Otto: High-Efficiency 200-Watt, 12-Gigahertz Traveling Wave Tube. NASA TN D-7709, 1974.

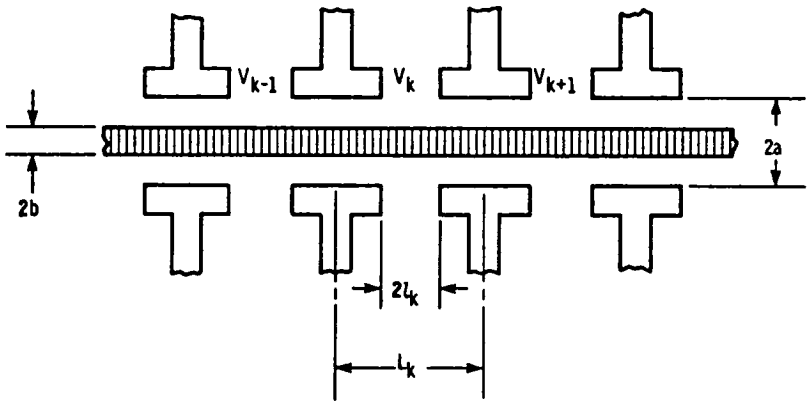

Figure 1. - Model of coupled-cavity traveling wave tube.

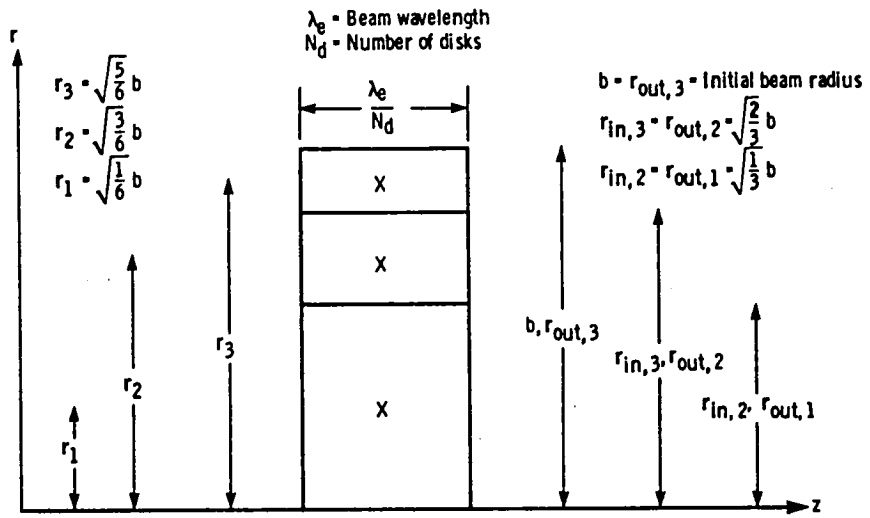

Figure 2. - Initial ring configuration for R = 3. r_j = centroid radius of j^{th} ring, j = 1, 2, 3; $r_{in,j}$ = inner radius of j^{th} ring, j = 1, 2, 3; $r_{out,j}$ = outer radius of j^{th} ring, J = 1, 2, 3.

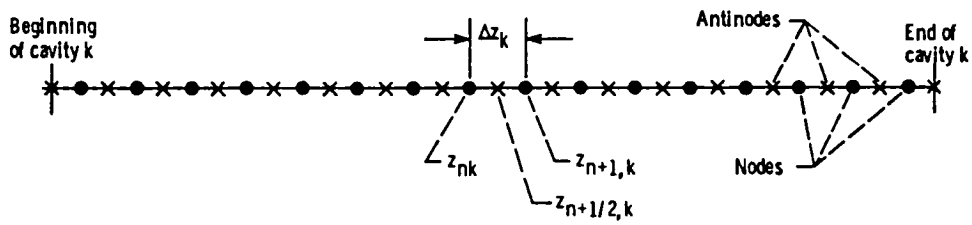

Figure 3. - Nodes and antinodes for cavity k.

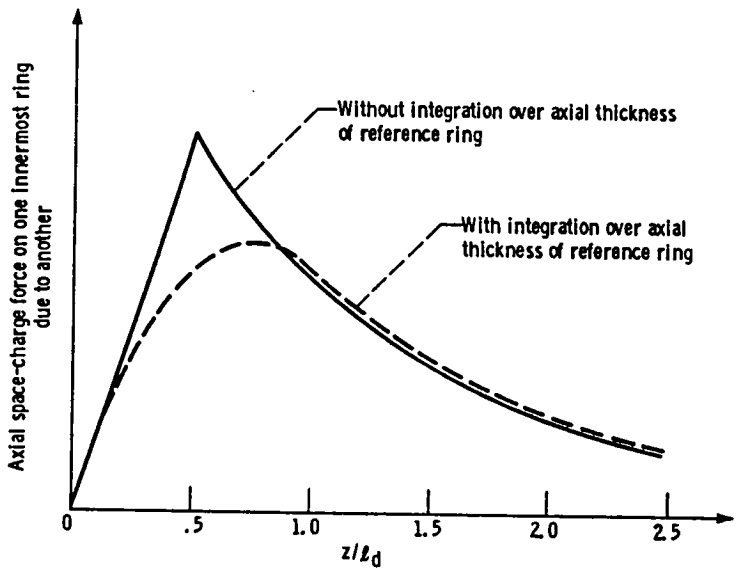

Figure 4. - Axial space-charge force on one innermost ring due to another as a function of normalized axial separation distance; $\ell_d/a = 1/3$.

Comparison of R-tables model to R^2-tables model of space charge forces. Consider 3 rings, all at same axial position, and all having their initial dimensions. Beam radius = 0.7 x tube radius. Innermost ring is ring #1, etc. Compare radial space charge forces. Axial thickness is $\lambda_e/24$.

Force on ring #	Due to ring #	R^2-tables model	R-tables model
1	1	1.171	1.184
1	2	-0.321	-0.330
1	3	-0.129	-0.133
		0.721	0.721
2	1	1.345	1.274
2	2	0.504	0.544
2	3	-0.371	-0.362
		1.478	1.456
3	1	0.783	0.766
3	2	1.082	1.056
3	3	0.377	0.401
		2.242	2.223

Figure 5. - Typical comparison of R^2-tables model to R-tables model.

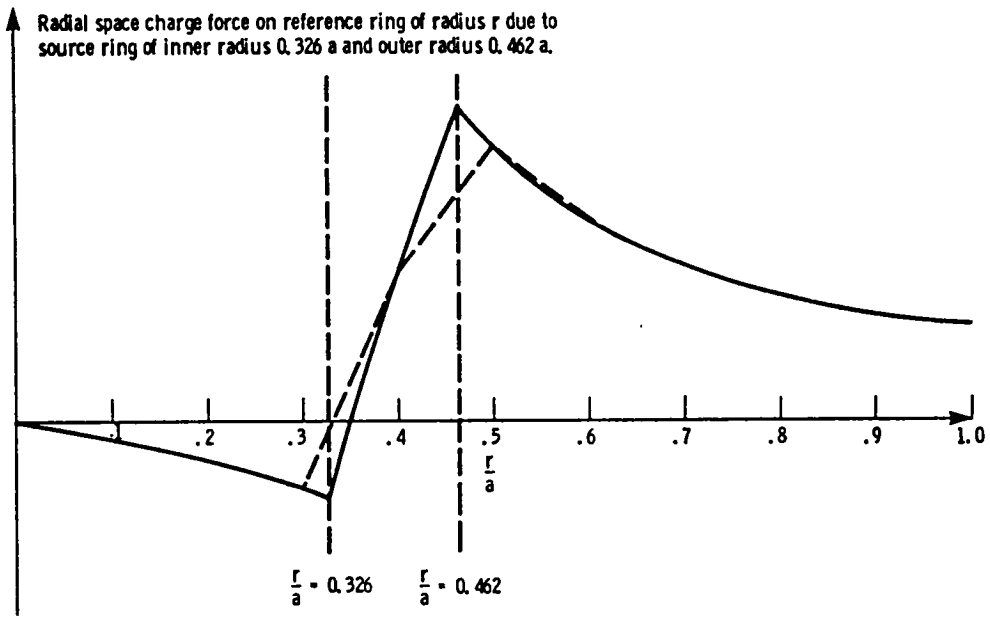

Figure 6. - Radial space charge force on a reference ring, due to one source ring, as a function of the reference ring's centroid radius.

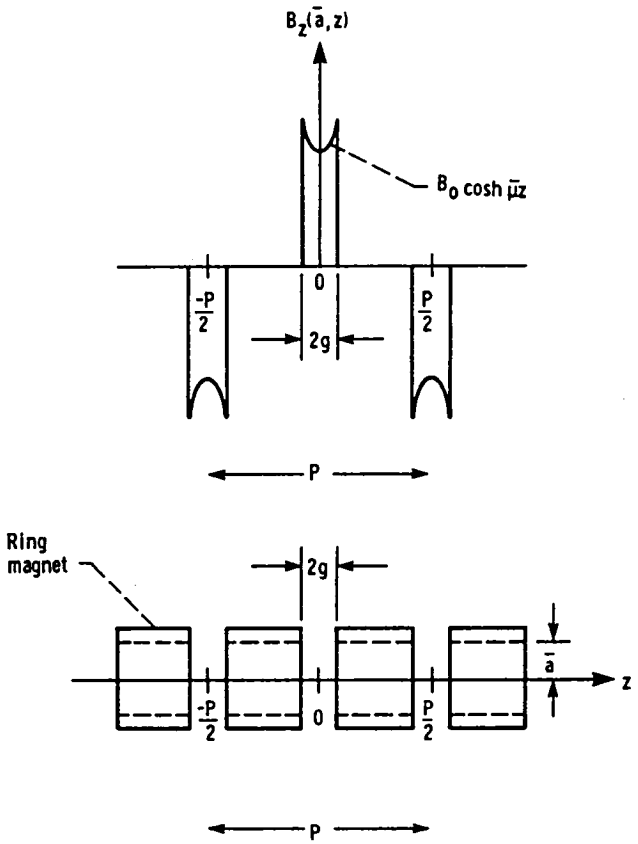

Figure 7. - Geometry and axial magnetic field for single period PPM focusing.

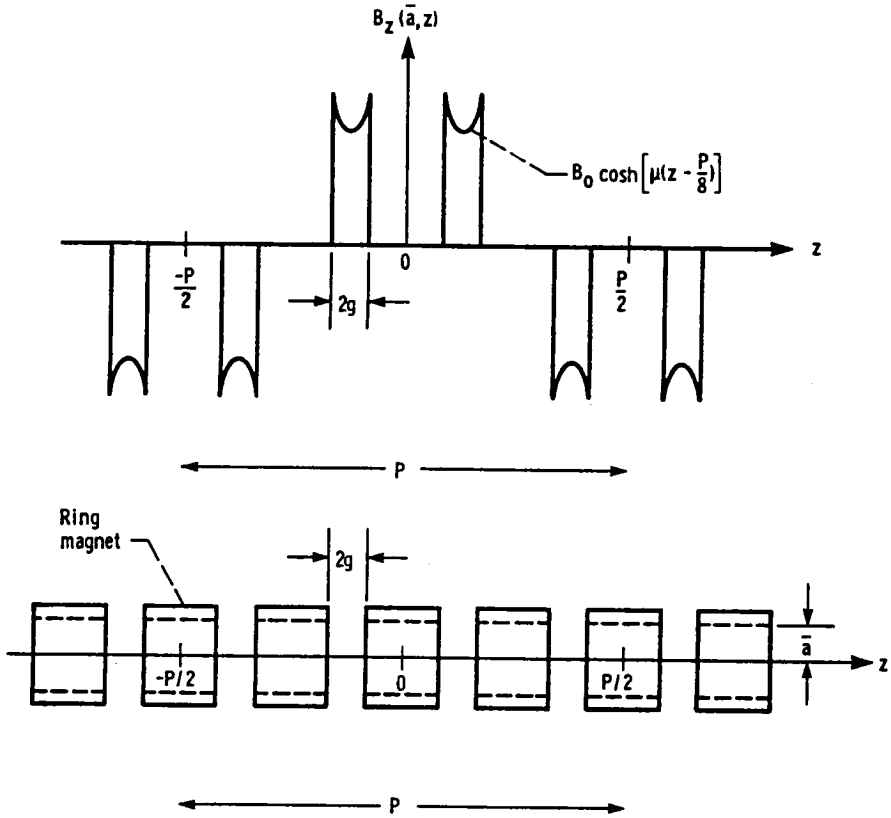

Figure 8. - Geometry and axial magnetic field for double period PPM focusing.

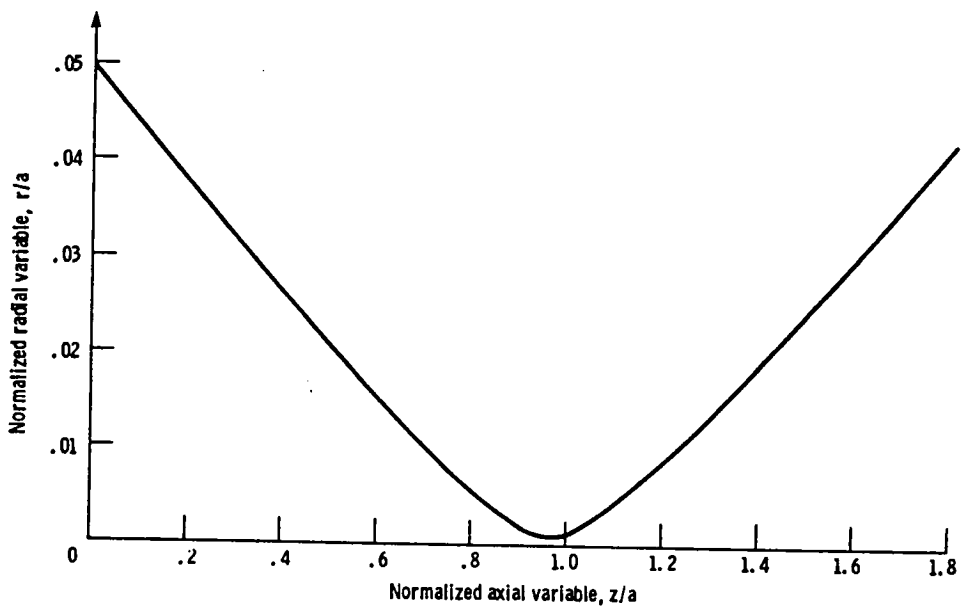

Figure 9. - Trajectory obtained from exact solution of equation r'' = K/r.

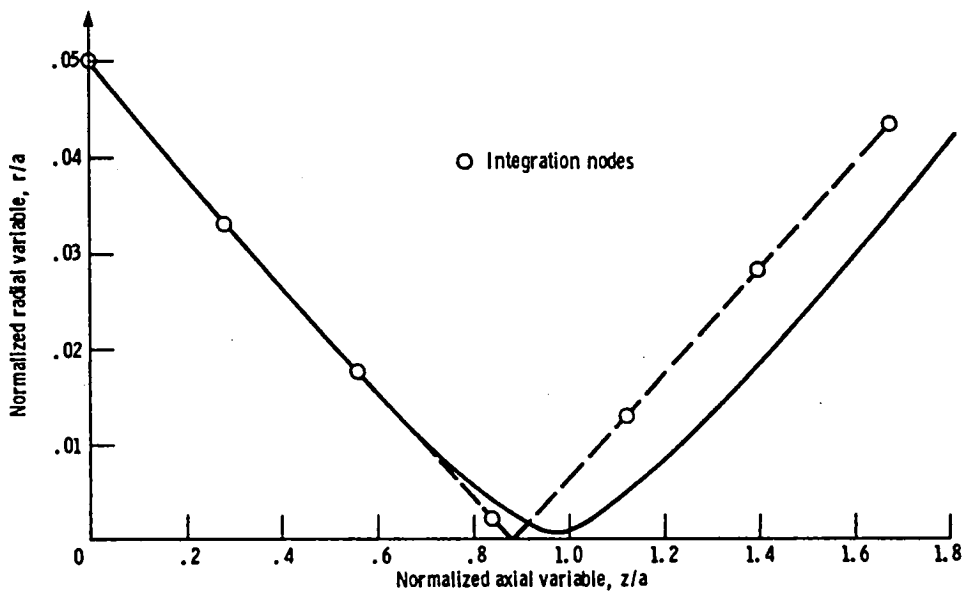

Figure 10. - Comparison of trajectory obtained from exact solution of equation r'' = K/r to the trajectory obtained from model used in computer program.

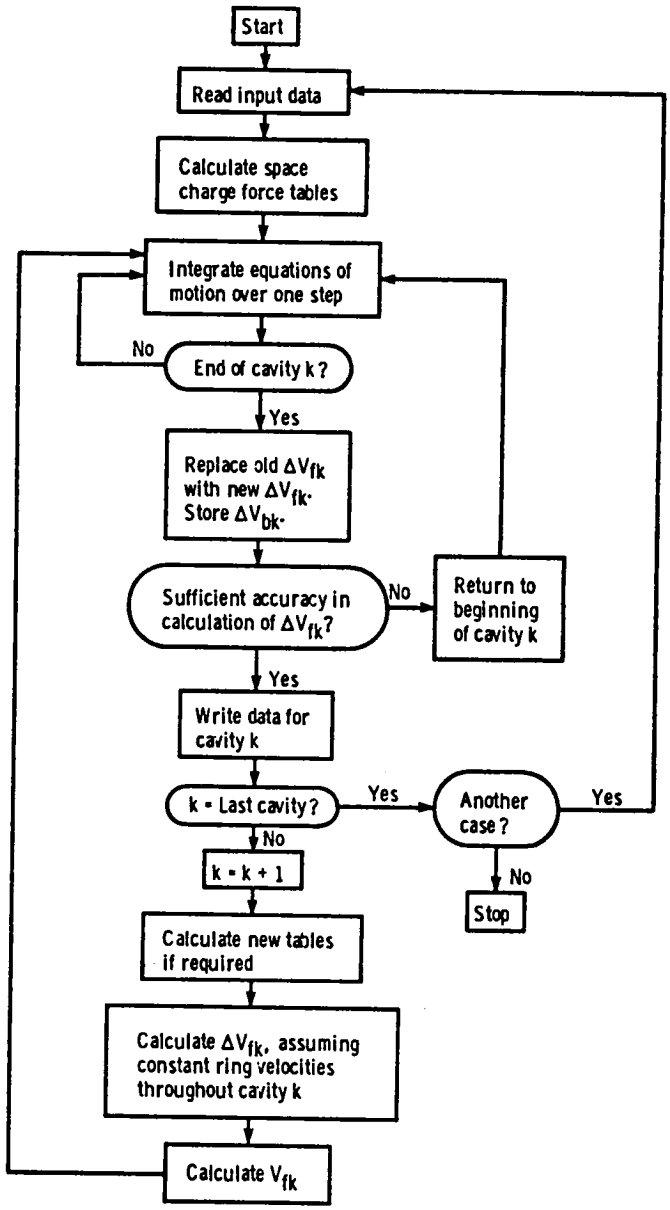

Figure 11. - Flow chart for computational procedure.

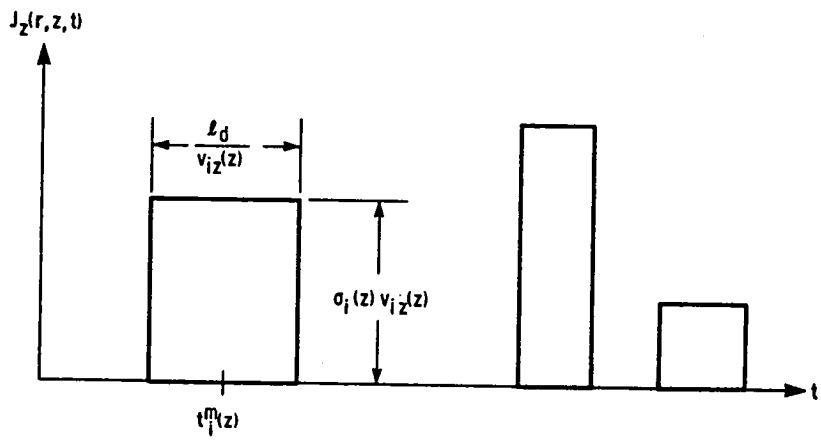

Figure 12. - Current density $J_z(r,z,t)$ as a function of t for some fixed r and z.

1. Report No.	2. Government Accession No.	3. Recipient's Catalog No.
NASA CR-168269		

4. Title and Subtitle	5. Report Date
Users' Manual for Computer Program for Three-Dimensional Analysis of Coupled-Cavity Traveling Wave Tubes	January 1984
	6. Performing Organization Code

7. Author(s)	8. Performing Organization Report No.
Thomas A. O'Malley	E-1930
	10. Work Unit No.

9. Performing Organization Name and Address	11. Contract or Grant No.
Analex Corporation 21000 Brookpark Road Cleveland, Ohio 44135	NAS 3-23293
	13. Type of Report and Period Covered
	Contractor Report

12. Sponsoring Agency Name and Address	14. Sponsoring Agency Code
National Aeronautics and Space Administration Washington, D.C. 20546	506-58-22

15. Supplementary Notes

Final report. Project Manager, Raymond W. Palmer, Space Communications Division, NASA Lewis Research Center, Cleveland, Ohio 44135.

16. Abstract

The use of the coupled-cavity traveling wave tube for space communications has led to an increased interest in improving the efficiency of the basic interaction process in these devices through velocity resynchronization and other methods. To analyze these methods, we have recently developed a flexible, three-dimensional, axially-symmetric, large-signal computer program for use on the IBM 370 time-sharing system. The present report is a users' manual for this program.

17. Key Words (Suggested by Author(s))	18. Distribution Statement
Computer program Three-dimensional analysis Coupled cavity TWT	Unclassified - unlimited STAR Category 33

19. Security Classif. (of this report)	20. Security Classif. (of this page)	21. No. of pages	22. Price*
Unclassified	Unclassified	59	A04

*For sale by the National Technical Information Service, Springfield, Virginia 22161

National Aeronautics and
Space Administration

Washington, D.C.
20546

Official Business
Penalty for Private Use, $300

SPECIAL FOURTH CLASS MAIL
BOOK

Postage and Fees Paid
National Aeronautics and
Space Administration
NASA-451

NASA

POSTMASTER: If Undeliverable (Section 158
Postal Manual) Do Not Return